NAVAL POSTGRADUATE SCHOOL
Monterey, California

UNITED STATES NAVY
NAVAL POSTGRADUATE SCHOOL

DTIC
ELECTE
JUL 17 1991
S B D

THESIS

THE NATURE OF THE PROPAGATION OF SEA
BREEZE FRONTS
IN CENTRAL CALIFORNIA

by

Joseph A. Yetter Jr.

September 1990

Thesis Advisor   William J. Shaw

Approved for public release; distribution is unlimited.

91-04986

REPORT DOCUMENTATION PAGE

1a Report Security Classification Unclassified		1b Restrictive Markings			
2a Security Classification Authority		3 Distribution Availability of Report			
2b Declassification Downgrading Schedule		Approved for public release; distribution is unlimited.			
4 Performing Organization Report Number(s)		5 Monitoring Organization Report Number(s)			
6a Name of Performing Organization Naval Postgraduate School	6b Office Symbol (if applicable) 35	7a Name of Monitoring Organization Naval Postgraduate School			
6c Address (city, state, and ZIP code) Monterey, CA 93943-5000		7b Address (city, state, and ZIP code) Monterey, CA 93943-5000			
8a Name of Funding Sponsoring Organization	8b Office Symbol (if applicable)	9 Procurement Instrument Identification Number			
8c Address (city, state, and ZIP code)		10 Source of Funding Numbers			
		Program Element No	Project No	Task No	Work Unit Accession No

11 Title (include security classification) THE NATURE OF THE PROPAGATION OF SEA BREEZE FRONTS IN CENTRAL CALIFORNIA

12 Personal Author(s) Joseph A. Yetter Jr.

13a Type of Report Master's Thesis	13b Time Covered From To	14 Date of Report (year, month, day) 1990, September	15 Page Count 78

16 Supplementary Notation The views expressed in this thesis are those of the author and do not reflect the official policy or position of the Department of Defense or the U.S. Government.

17 Cosati Codes			18 Subject Terms (continue on reverse if necessary and identify by block number)
Field	Group	Subgroup	LASBEX, Lidar, Sodar

19 Abstract (continue on reverse if necessary and identify by block number)

An examination is made of the nature of propagation of sea breeze fronts in central California. From 15 to 30 September, 1987, the Land Sea Breeze Experiment (LASBEX) provided a series of meteorological observations including sodar, lidar, rawinsonde, radiosonde and surface observations. Surface observations of opportunity were also available from local marine labs and airports.

Using a very simple linear model, the speed and direction of the sea breeze front is investigated. The speed of frontal propagation varied from 1 m s to 3 m s. A correlation between the speed of frontal propagation and estimated surface heat flux is observed. The direction of frontal propagation tends to be up valley. Comparison of the frontal propagation vector with stations in the southern portion of Monterey Bay shows that the front is curved on the mesoscale.

20 Distribution Availability of Abstract ☒ unclassified unlimited ☐ same as report ☐ DTIC users	21 Abstract Security Classification Unclassified	
22a Name of Responsible Individual William J. Shaw	22b Telephone (include Area code) (408) 646-2044	22c Office Symbol 63Sr

DD FORM 1473,84 MAR 83 APR edition may be used until exhausted security classification of this page
All other editions are obsolete

The Nature of the Propagation of Sea Breeze Fronts
in Central California

by

Joseph A. Yetter Jr.
Lieutenant, United States Navy
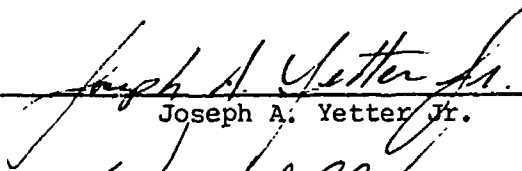B.S., California State College, PA, 1982

Submitted in partial fulfillment of the
requirements for the degree of

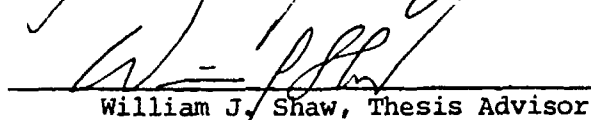MASTER OF SCIENCE IN METEOROLOGY AND OCEANOGRAPHY
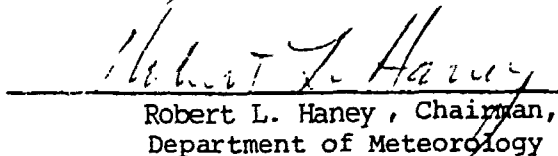
from the

NAVAL POSTGRADUATE SCHOOL
September 1990

Author: _____
Joseph A. Yetter Jr.

Approved by: _____
William J. Shaw, Thesis Advisor

_____
Philip A. Durkee, Second Reader

_____
Robert L. Haney , Chairman,
Department of Meteorology

ABSTRACT

An examination is made of the nature of propagation of sea breeze fronts in central California. From 15 to 30 September, 1987, the Land/Sea Breeze Experiment (LASBEX) provided a series of meteorological observations including sodar, lidar, rawinsonde, radiosonde and surface observations. Surface observations of opportunity were also available from local marine labs and airports.

Using a very simple linear model, the speed and direction of the sea breeze front is investigated. The speed of frontal propagation varied from 1 m/s to 3 m/s. A correlation between the speed of frontal propagation and estimated surface heat flux is observed. The direction of frontal propagation tends to be up valley. Comparison of the frontal propagation vector with stations in the southern portion of Monterey Bay shows that the front is curved on the mesoscale.

Accession For

NTIS GRA&I	☑
DTIC TAB	☐
Unannounced	☐
Justification	

By_____
Distribution/
Availability Codes

| Dist | Avail and/or Special |
| A-1 | |

TABLE OF CONTENTS

LIST OF TABLES

LIST OF FIGURES

ACKNOWLEDGMENTS

I. INTRODUCTION

A. LAND-SEA BREEZE DESCRIPTION

For centuries, inhabitants of coastal regions have observed the inland push of cool, marine air in the daytime and offshore flow at night. This regime of diurnally reversing winds is referred to as the land-sea circulation. Fig. 1 provides a schematic representation of the sea breeze circulation. During the course of the day, differential surface heating initiates the thermally direct land-sea breeze circulation. Incoming solar radiation warms the land more than the adjacent water. The resulting temperature contrast produces a slight variation in pressure. The isobaric surfaces bend upward over the land, producing an upper-level high. The upper-level air flows seaward increasing the surface pressure over the water. The air over the water moves from the sea toward the land in response to the resultant pressure gradient.
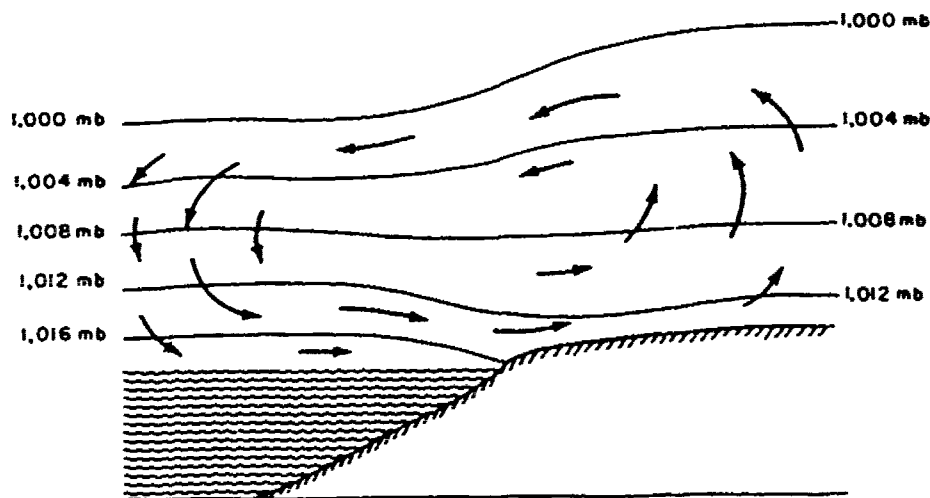
Fig. 1. Sea Breeze Schematic: Isobars are initially horizontal (from Blair and Fite 1965).

1

The thermally direct land breeze circulation is the nighttime counterpart of the sea breeze. Nocturnal cooling results in the evolution of a low-level pressure gradient from land to water and the air flows offshore. As previously stated, the generation mechanism is similar to the sea breeze but operates in a reverse manner. The land breeze is usually less developed than the sea breeze; it is shallower, slower and has less horizontal extent.

Defined as the leading edge of inland-penetrating marine air, the sea breeze front is the most dramatic feature of the sea breeze circulation (Fosberg and Schroeder, 1966). The sea breeze front is generally marked by low-level convergence, a temperature decrease, an increase in humidity, and a substantial change in wind direction. However, there are times when a sea breeze front is not accompanied by any noticeable change in wind direction. In this case, the front is still distinguishable by a temperature decrease and a humidity increase as it passes (Atkinson, 1981).

B. LAND-SEA BREEZE EXPERIMENT (LASBEX)

LASBEX was conducted in the Monterey Bay area to investigate characteristics of central California's sea breeze circulation, its microstructure and its relationship to aerosol distributions. From 15 September to 30 September 1987, data were collected across the mouth of the Salinas Valley. Numerous meteorological sensing systems were employed, including a doppler acoustic sounder (SODAR), a doppler lidar, rawinsondes, radiosondes, surface meteorological systems and satellites.

Fig. 2, a wind direction time height cross section from Fagan (1988), illustrates the sharp character of the sea breeze front. However,

2

single station observation not provide any information concerning the spatial characteristics of the sea breeze front. Using the entire suite of surface measurements, this study will examine the spatial characteristics of the sea breeze circulation indigenous to California's central coast.

C. SIGNIFICANCE

The land-sea breeze circulation is observable in coastal regions of all latitudes. Since coastal regions tend to be densely populated, the sea breeze circulation is in constant interaction with mankind. As the sea breeze pushes onshore, it has an impact on the air quality through horizontal transport of pollutants. Local agriculture tends to evolve around the land-sea breeze circulation patterns. Recreationally, the sea breeze circulation is useful to hang gliding and sailing. Probably one of the most noticeable impacts of the sea breeze is the moderating effect it has on observed temperatures. In parts of California, where the sea breeze is a daily occurrence, afternoon temperatures are on the average lower than they otherwise would be (Blair and Fite, 1965). The sea breeze is also an integral part of the prediction equation in the forecasting of fire-weather conditions and radioactive fallout patterns (Fosberg and Schroeder, 1966, Schoeder et. al., 1967). The movement of marine air across coastal boundaries can also significantly modify the refractive character of the atmosphere. As the sea breeze penetrates inland the changes in atmospheric humidity produce variations in electromagnetic propagation. As the boundary layer height increase an associated increase in the trapping of electromagnetic energy is observed. This is important in evaluating the propagation of electromagnetic energy. Through aerosol dispersion, land-sea breeze circulations can affect satellite imaging capabilities by changing the extinction coefficient of the local atmosphere.

3
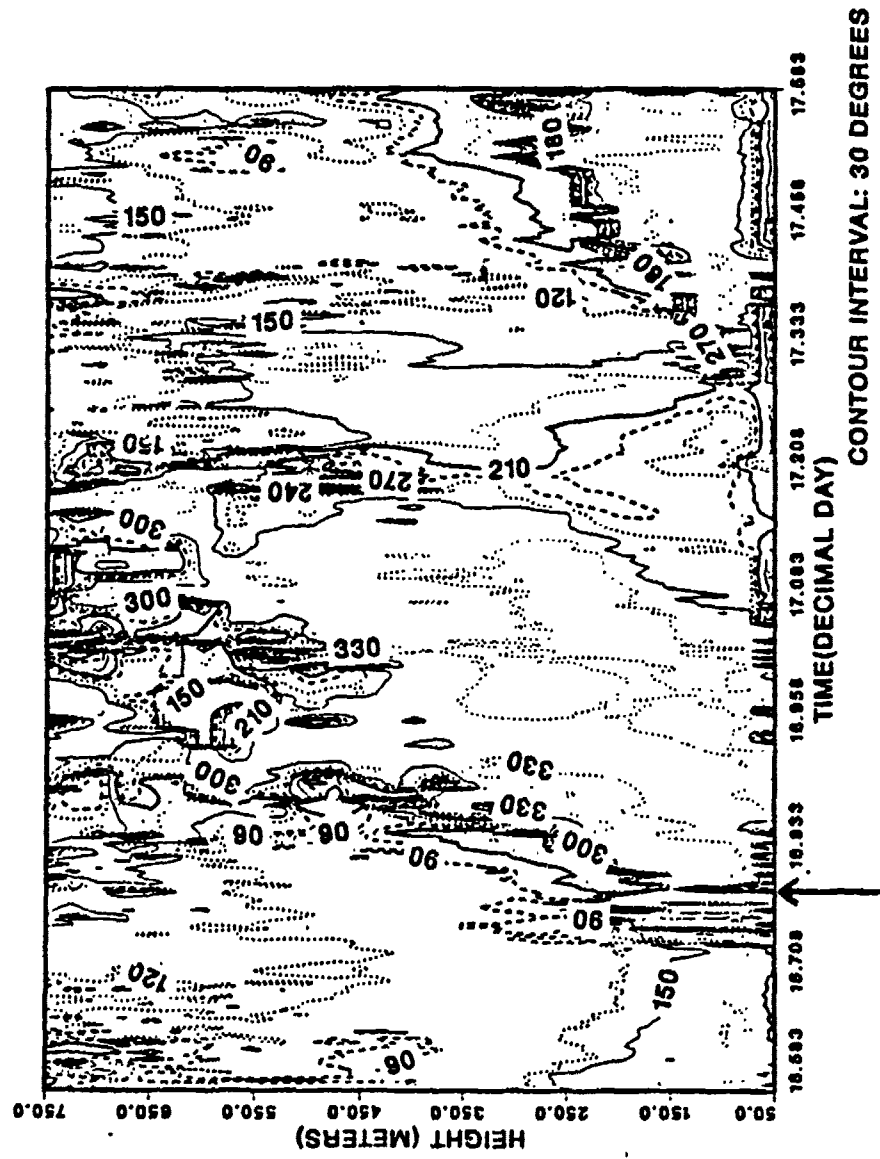
Fig. 2   24 Hour Directional Plot for 16 September 1987:   The sea breeze
        is indicated by the arrow (from Fagan 1988).

4

D. REVIEW OF PREVIOUS WORK

1. Models

Walsh (1974) provides an analytical look at the sea breeze circulation using a two dimensional model. Since the sea breeze is a phenomenon of the lower atmosphere, Walsh's model employed linearized Boussinesq equations which include rotation of the earth, vicosity of the circulation and mean stratification of the atmosphere. Walsh used a surface temperature function to prescribe the thermal forcing of the model. The results were divided into two categories, symmetrical and asymmetrical circulations. A symmetrical circulation pattern produced a concentration of high velocities near the coastline. This was considered to be a realistic result by Walsh. With the inclusion of advection the circulation became asymmet- ·l resulting in diminished coastline velocities. The latter situatı tends to suggest a sea breeze front will form. Through vertical : flux calculations, Walsh explored the importance of the sea breeze circulation on the global heat budget. He concluded that the sea breeze scenario is responsible for 1 to 3 percent of the global average of vertical heat flux.

Rotunno (1983) provided a historical review of various linear models applied to land-sea breeze theory. From this review, a hydrostatic, inviscid linear sea breeze model was developed. Using periodic forcing, the model evaluated the behavior of the sea breeze circulation in response to the variation of the coriolis force, f , with respect to the frequency of the diurnal heating cycle, w. For the case of $f > w$ (latitudes greater than 30°), the coriolis force decelerates the sea breeze circulation. For $f < w$, Rotunno found that the circulation was 180° out of phase with the heating. This resulted from the coriolis

5

force and the buoyancy force in the circulation equation being in phase. Although this result is counter-intuitive, by explicitly including friction, letting $(F^x, F^y) = -a(u,v)$ and $F^z = 0$, a more realistic behavior would result.

Pielke (1984) examined the sea breeze circulation over flat terrain. His model investigated the effect of variations in the local wind pattern on the sea breeze circulation. The synoptic flow was classified as weak, less than or equal to 6 m/s, or strong for flow greater than 6 m/s. When the prevailing onshore flow is weak, a tight, well-defined sea breeze circulation is produced. With stronger onshore flow the large pressure gradient can not develop due to the swift inland movement and subsequent greater warming of the marine air. The stronger synoptic flow results in a more diffuse sea breeze circulation. Pielke examined the magnitude of the effect of a particular horizontal temperature gradient on local wind patterns. He concluded that horizontal gradients of less than 10 W/m^2 per 30 km slightly influence the local wind patterns. Horizontal gradients of 100 W/m^2 or 1000 W/m^2 per 30 km produce significant and very pronounced variations to local wind patterns.

In 1987, Yan and Anthes employed a two-dimensional, nonlinear sea breeze model integrated over a five day period to evaluate the effect of variations in latitude on sea breeze circulations. The model was run at the equator, 20° N., 30° N., and 45° N. The observational day was divided into two parts. The first part was considered to be marked by strong heating which produced large friction and small static stability values. Under these conditions, Yan and Anthes surmised that

the dominance of the pressure gradient force associated witn the strong temperature contrast will result in a similar development cf sea breeze circulations at all latitudes. The rest of the observational day was marked by a weakening of the pressure gradient and frictional forces and static stability increases which resulted in the domination of the coriolis force (except near the equator). Therefore, circulations which were initiated in similar fashion actually evolved differently based on latitudinal location. Since the variation of the coriolis force is an important factor in the rate of rotation of the horizontal wind, Yan and Anthes conclude that perhaps the coriolis force is more important than the day to night reversal of the horizontal temperature gradient in the development of land breezes.

Using a simple sea breeze model, Hsu (1988) examined the sea breeze circulation along the Texas coast. From Bjerknes's circulation theorem, neglecting friction, the sea breeze intensity should increase until the temperature difference between the land and sea changes from positive to negative. By including friction, the sea breeze intensity maximum would be expected to occur while the land is still warmer than the sea since a positive temperature difference is required to overcome the friction. From measurements along the Texas coast, Hsu's model produced a mean sea breeze circulation speed of 8.8 m/s perpendicular to the coast. This result agreed well with actual sea breeze circulation speed observations of 8 m/s at the time of maximum sea breeze. This is greater than the speed of propagation of the sea breeze front.

Feliks (1988) analytically solved the nonlinear, nonhydrostatic equations of motion in order to investigate the inland penetration of the sea breeze circulation. Feliks assumed a constant frontal speed and the maintenance of the frontal structure in this study. The result was that the square of the frontal speed relative to the synoptic wind is proportional to the mean drop of potential temperature over the frontal area multiplied by the frontal height. From this, Feliks concluded that fronts with smaller temperature drops can propagate faster if the frontal radius is sufficiently large. Feliks also used the vorticity equation in observations of frontal propagation.

$$\frac{\partial \zeta}{\partial t} + u \frac{\partial \zeta}{\partial x} + w \frac{\partial \zeta}{\partial z} = \frac{\partial \sigma}{\partial x}$$

$$\zeta = \frac{\partial w}{\partial x} - \frac{\partial u}{\partial z} = \nabla^2 \psi$$

The terms of interest were the nonlinear advection term, $-J(\psi, \zeta)$, and the horizontal gradient of buoyancy, $\frac{\partial \sigma}{\partial x}$. Feliks found that the buoyancy term will always tend to propagate the front inland. A positive nonlinear advection term will also propagate the front inland. A negative nonlinear advection term decreases the vorticity and inhibits frontal propagation.

Dalu and Pielke (1989) employed an extension of Rotunno's model to include non-periodic forcing. With this change, they examined variations in sea breeze intensity and inland penetration as a function of latitude. Using equatorial and mid-latitude values of the coriolis force, this study examined the development of the sea breeze circulation. The principal conclusion was that both inertia and friction are

important contributors to sea breeze intensity and inland penetration.
However, in lower latitudes, where the coriolis force is negligible,
fricition is the controlling factor of sea breeze intensity and
penetration.

2. Sea Breeze Observations

Wexler (1946) and, more recently, Atkinson (1981) provide basic
reviews of the evolution of the land-sea breeze circulation pattern.
Both authors discuss the influence of the gradient wind, topography,
and atmospheric stability on the development of the sea breeze
circulation.

The direction of the gradient wind can either help or hinder
the development of the sea breeze. If the gradient flow is onshore,
the differential heating along the coast may be hampered, thereby
reducing the chance of sea breeze development. However, sea breezes
do develop with onshore gradient winds. On days having light, onshore
gradient winds, the development of the sea breeze circulation appears
to occur earlier in the day. Since the thermal and pressure gradients
necessary for the development of the sea breeze are pushed out to sea,
offshore gradient winds can delay the sea breeze until later in the
day, decrease the inland extent, and cause a much earlier retreat. It
should be noted that the term development does not refer to th· ·~t·ial
set up of the circulation pattern but to the movement of the front
across the coastline. Gradient winds which flow parallel to the
coastline do not hinder the development of the sea breeze circulation
(Frizzola and Fisher, 1963).

Terrain variations and vegetation cover can influence the development of the sea breeze circulation. Coastal ranges, depending on their orientation, can either accentuate or retard the sea breeze circulation. Natural gaps in the ranges can allow for deeper inland penetration of the sea breeze. By superimposing the sea breeze on up-slope or up-valley flows much greater wind velocities are achieved. The vegetation cover influences the rate of heating of the land surface. The more barren the land the quicker the heating process and the stronger the sea breeze circulation.

Atmospheric stability is a key factor in the determination of the time of onset of the sea breeze. During periods of strong surface heating the lower atmosphere becomes unstable. It is during this period that the penetration of the sea breeze circulation is most likely. With the inversion layer acting as a strong damping mechanism, a stable atmosphere will inhibit the vertical extension of the sea breeze circulation. Less stable air would encourage the extension and intensification of the sea breeze circulation.

Fosberg and Schroeder (1966) investigated the penetration of marine air in central California. They analyzed data acquired during July and August, 1961. The initial speed of advance of the marine air was determined to be 5 to 7 m/s. As the day progressed, the speed of advance decreased to 1 to 2 m/s, eventually dissipating between 1700 and 1800 Pacific Standard Time (PST). They classified sea breeze days according to the maximum temperature at Sacramento. The survey days were separated into one of three divisions: 1) cool days with temperatures of 32°C or less, 2) intermediate days with temperatures

between 33°C and 37°C, and 3) warm days with temperatures of 38°C or higher. Fosberg and Schroeder found the role of topography in channeling and deflecting the sea breeze was noticeable on warm days and to a lesser extent on cool days.

In 1967 Schroeder et al. provided a review of various studies dealing with the penetration of marine air along the Pacific coast. They recognized three types of sea breeze fronts. First, the classical or air mass sea breeze front is marked by a sharp decline in temperatures, increases in humidity and wind velocity changes. The wind shift line is the second type of sea breeze front identified. This is a thermally modified air mass front. The third sea breeze front recognized by Schroeder et al. was characterized by sustained cooling and rises in humidity without a wind shift line. This was referred to as a cool change front. The varying character of the sea breeze front has been attributed to differing gradient flow. For example, Frizzola and Fisher (1963) found the classical front with associated sharp discontinuities was a result of the gradient flow opposing the sea breeze direction. During LASBEX both classical and cool change sea breeze fronts were observed.

Olsson et al. (1973) provided observational information on marine air penetration in western Oregon. Sea breeze circulations were observed during the summers of 1969 and 1970. Both periods were dominated by high pressure off the coast which resulted in an onshore flow pattern. By examining surface temperature records and shifts in wind direction at Grand Ronde, Perrydale and Salem, they calculated a sea breeze penetration rate of 5 m/s. By examining the wind component

perpendicular to the leading edge of the marine air, Olsson et al. estimated frontal vertical velocities of 0.4 m/s. They concluded that the penetration of the sea breeze inland is a result of the interaction between the sea breeze flow, topographic winds and the prevailing synoptic flow. For example, if either topographic winds or synoptic winds were opposi.., the sea breeze flow and were strong enough they could result in eit. :r a slower penetration rate or no inland penetration at all.

In 1973, Johnson and O'Brien examined sea breeze events along the Oregon coast. Their observations were made in August, 1972. The synoptic pattern was once again dominated by the east P.cific anticyclone. Johnson and O'Brien observed that as the day progressed the speed of advance of the sea breeze decreased. They concluded by making the following observations: 1) at more than 60 km inland a sea breeze front was evident; 2) the sea breeze front was followed by a distinct wind maxiumum; 3) the onshore flow was restricted to the marine layer and 4) the return flow above the inversion appears in surges. The surging character was probably in response to the surges observed in the sea breeze itself.

Simpson et al. (1977) statistically analyzed the inland penetration of sea breeze fronts in England. The analyzed data covered a twelve year period from 1962 through 1973. During this period, they found that with onshore winds prevailing, the sea breeze fronts penetrated 30 to 40 km inland. In a few extreme instances, the sea breeze front was distinguishable up to 100 km inland. Simpson et al. observed an average speed of advance of 2 m/s for sea breeze fronts during this study.

The following chapters will discuss the Land-Sea Breeze Experiment and the use of a simple linear model to investigate the propagation inland of the sea breeze front.

II. THE EXPERIMENT

A. LOCATION

From 15 to 30 September 1987, the Land-Sea Breeze Experiment
(LASBEX) was conducted on California's central coast. The observational
systems which composed LASBEX were operated by the Naval Postgraduate
School (NPS), Naval Environmental Prediction Research Facility (NEPRF)
which was recently renamed Naval Oceanographic and Atmospheric Research
Laboratory (NOARL) Monterey Detachment, NOAA's Wave Propagation
Laboratory (WPL) and Louisianna State University (LSU). The recording
stations were situated around the Monterey Bay to take extensive
measurements of the sea breeze penetration into the Salinas Valley.
Supplemental data were acquired from local marine laboratories and
airports in the region. By combining the data sets a fairly extensive
coverage pattern across the Monterey Bay/Salinas Valley was achieved.
Table 1 provides a list of the observing systems deployed during LASBEX
and Table 2 provide a list of the observing systems of opportunity.

The Salinas Valley, situated between the Gabilan and Sierra De
Salinas mountain ranges, is about 20 km wide at the entrance and extends
roughly 140 km to the southeast at approximately 140°. The location of
the area studied, positions of observing sites in kilometers north and
east of Moss Landing and local topography are illustrated in Fig. 3.

B. DOPPLER LIDAR

The NOAA WPL pulsed Doppler lidar uses backscattered laser energy
to measure radial wind velocities and extinction in optically clear air.

14

Typical range and transverse resolutions are 300 m and about 1 m

respectively (Intrieri et al., 1990). The use of a narrow optical

beam allows the lidar to scan close to the sea and land surface,

allowing for measurements very near terrain features.

Table 1. LASBEX OBSERVING SYSTEMS

System	Operator	Variable Measured	Resolution
Doppler Lidar	NOAA WPL	Doppler Velocities	300 m Horizontal
Sodar: Doppler, Monostatic	NPS/NEPRF	Wind Profiles	25 m Vertical
Rawinsondes	NPS	P, T, RH, Wind Speed, Wind Direction	50 m Vertical
Radiosondes	LSU	P, T, RH	25 m Vertical
Surface Stations	NPS/NEPRF	P_s, T_s, RH_s, Wind Speed, Wind Direction	20 s
Satellites: AVHRR, GOES		Aerosols, Weather System Movement	1.1 km for AVHRR, 1 km for VIS-8 km for IR for GOES

Table 2. OBSERVING SYSTEMS OF OPPORTUNITY

Station	Variables Measured	Resolution
Marina Beach (Scripps Institute of Oceanography)	Wind Speed, Wind Direction	8 s
Moss Landing Marine Laboratory	P_s, T_s, RH_s, E, Wind Speed, Wind Direction	5 min
Monterey Bay Aquarium	P_s, T_s, RH_s, E, Wind Speed, Wind Direction	5 min
Monterey Airport	P_s, T_s, RH_s, Wind Speed, Wind Direction	Hourly
Salinas Airport	T_s, P_s, RH_s, Wind Speed, Wind Direction	Hourly
Fritzsche Field	P_s, T_s, RH_s, Wind Speed, Wind Direction	Hourly

The lidar was operated in three different modes: 1) low elevation angle

plan-position indicator (PPI), which provides horizontal wind and aerosol

information; 2) range-height indicator (RHI), which provides vertical

structure information; and 3) the wind profiling mode which scanned

the radial wind field (Intrieri et al., 1990). The lidar was located

at the mouth of the Salinas Valley during LASBEX, approximately

1.5 km from the coast.
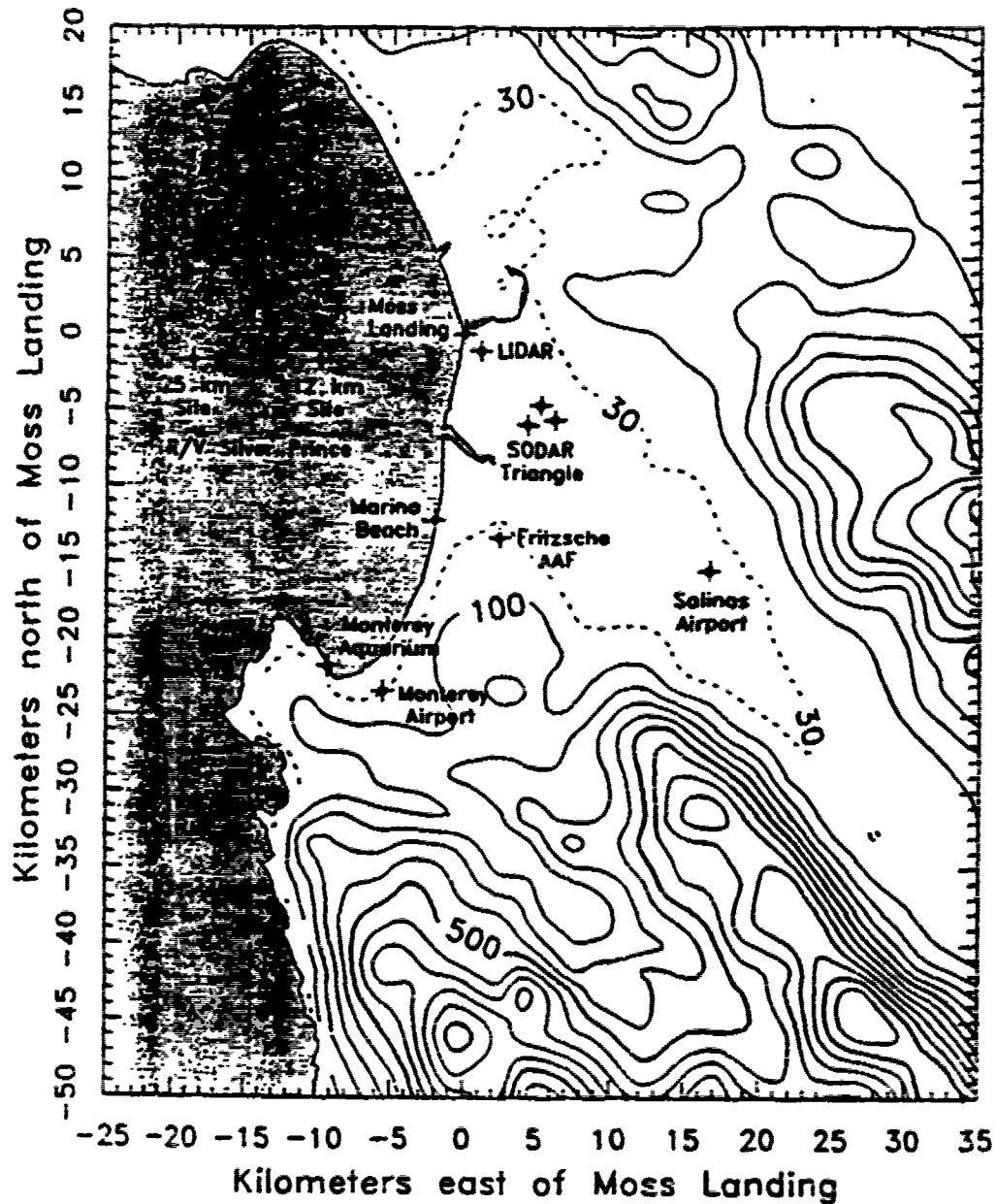
Fig. 3. Location of Recording Stations: Coordinates are in kilometers
        from Moss Landing. Elevations are in meters (from Shaw and
        Lind, 1989).

16

C. SODAR

1. Doppler Sodar

During LASBEX, three sodars were deployed. As Fig. 3 illustrates, the sodars were situated in a triangular pattern measuring approximately 1 km a side. NPS and NEPRF personnel operated the sodars. The primary sodar site at the northern vertex of the sodar triangle was operated at 1600 Hz by NPS personnel. The tri-axis phased array doppler system used backscattered acoustic energy to measure turbulent fluctuations within the atmosphere. Cycling through its axes every 30 seconds, the sodar used ten cycle averages to produce wind profiles at 5 minute increments. Using Fast Fourier Transform processing techniques, the sodar calculated mean wind components, variances of each component and an estimate of a temperature structure function c_T^2 from 50 to 750 meters with 25 meter resolution (Intrieri et al., 1990). Except for a few periods of power loss, the primary sodar site was in continuous operation from 16 September to 29 September 1987.

The second sodar site (sodar 2) was located at the eastern vertex of the sodar triangle. It was also operated by NPS personnel. Operating at 2000 Hz, sodar 2 used a complex covariance method to determine the wind components. This site was operational only from 25 September to 29 September, 1987.

2. Monostatic Sodar

Located at the western vertex of the triangle, the third sodar site (sodar 3) was operated by personnel from NEPRF. Operating at 5 kHz, the single-axis sodar provided high resolution (3.4m) data

(Intrieri et al., 1990). As a result of excessive ambient noise levels created by a nearby highway, the Sodar 3 was transferred to the lidar site on 25 September.

D. SURFACE MEASUREMENTS

1. LASBEX Surface Stations

Six surface meteorological stations, three operated by NPS and three operated by NEPRF, were used to measure surface pressure, air temperature, humidity, wind speed and wind direction at 20 second intervals. The stations deployed by NPS were located on board the R/V Silver Prince at approximately 5 meters above the water level, at the lidar site and at the primary sodar site. NEPRF operated surface stations at each vertex of the sodar triangle.

2. Surface Stations of Opportunity

Moss Landing Marine Laboratories (MLML) operated a continuous data acquisition system which measured wind speed, wind direction, relative humidity, solar irradiance, air temperature and barometric pressure. The sensors employed by this system are an Aerovane anemometer, a motor-aspirated, radiation-shielded thermistor and relative humidity sensor, an Epply star pyranometer and a calibrated pressure transducer. The instruments were located on the roof of the Moss Landing Marine Laboratories building at an elevation of 10 meters above mean sea level. The sensors are scanned and the data logged at 10 second intervals. Vector average winds and simple means of the other parameters are stored at 5 minute increments.

The Monterey Bay Aquarium employs an identical data acquisition system as MLML. The instruments were located on the aquarium's roof

18

at approximately 20 meters above mean sea level. The averaging and storing techniques are identical to Moss Landing Marine Laboratories.

During LASBEX Scripps Institute of Oceanography was operating a portable data acquisition system at Marina Beach. Wind speed and wind direction data were recorded every 8 seconds by the anemometer which was approximately 27 meters above mean sea level. These data were then stored in a condensed format on 9-track magnetic tape.

Two local airports and one military airfield take hourly observations of barometric pressure, air temperature, relative humidity, wind speed and wind direction. The data from Monterey Airport, Salinas Airport and Fritzsche Army Airfield (Ft. Ord) are routinely received and archived at the NPS Interactive Digital Environmental Analysis Laboratory (IDEA LAB).

E. UPPER AIR MEASUREMENTS

28 Rawinsondes and 27 radiosondes were used to gather thermodynamic information. The R/V Silver Prince which was chartered by NPS carried the VIZ W-8000RP+ rawinsonde system on board. Temperature, humidity and pressure were measured using a standard rod thermistor, carbon hygristor and an aneroid cell/baroswitch. The rawinsondes provided atmospheric sampling with 50 m vertical resolution. With the added capability of Loran-C time differencing, the rawinsondes were able to measure horizontal wind components. The rawinsondes were launched at 2 hour intervals and terminated at 500 mb. Due to limited funds, the R/V Silver Prince was chartered only during daylight hours and did not operate on weekends.

LSU personnel were in charge of launching the 27 land-based radiosondes. The radiosondes were launched at the primary sodar site and measured air temperature, humidity and pressure at 15 second intervals. The launches were timed to coincide with interesting changes in the local weather pattern as determined by the lidar.

F. SYNOPTIC SITUATION

LASBEX extended from 1200 PST 15 until 1300 PST 30 September 1987. The synoptic summary for this period will focus on the National Meteorological Center's (NMC) MSL surface pressure analysis.

The typical summer and early autumn weather pattern for California's central coast is a cyclone-anticyclone couplet. A subtropical high pressure system is present over the eastern north Pacific with an thermal low found over California's central valley. The subsidence associated with the subtropical high is responsible for the central coast's pattern of low clouds and fog at night and in the early morning. This synoptic pattern tends to spawn sea breeze circulations.

From NMC surface analyses, a time series of the central pressures for the eastern Pacific anticyclone and the inland thermal low is shown in Fig. 4. The anticyclone was relatively stationary and long lived with a fairly steady pressure field. Although the thermal low migrated northward, it appears to have a fairly steady pressure field. The associated troughing into northern California did increase during LASBEX. From 24 September to 26 September, the thermal low was deepening and the subtropical high was building. This resulted in a stronger pressure gradient over the coastal region.

From 16 September to 24 September high surface pressure prevail off the California coast. The combination of the subtropical high and the inland thermal low produced northerly winds between 5 and 10 knots of Oakland. Fig. 5 illustrates California's typical synoptic weather pattern. On 24 September a 1017 mb low pressure center developed at approximately 41.5°N., 131.0°W. Fig. 6 shows the surface pressure analysis for 24 September 1987. As the system progressed eastward, the usual seasonal configuration was disrupted. This resulted in 15 to 20 knot northerly winds. After 25 September, the anticyclone-cyclone configuration reestablished itself. This pattern was maintained throughout the rest of the observational period.
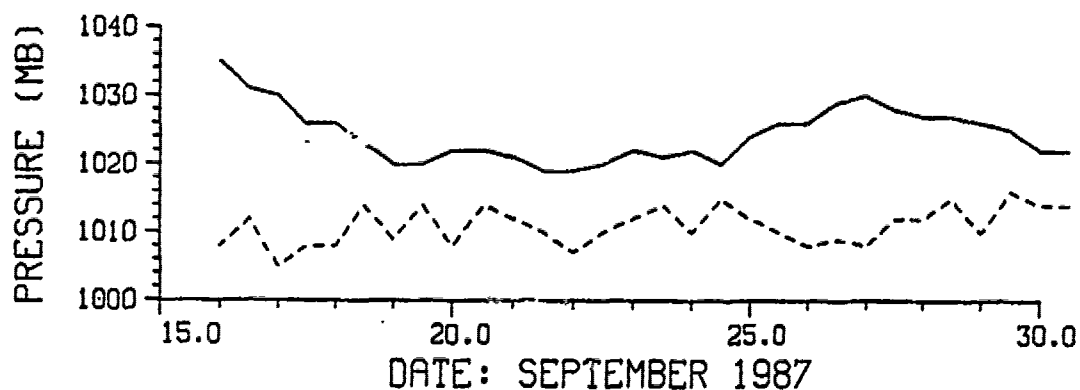
Fig. 4. Time series of central pressure of anticyclone (solid) and cyclone (dashed).

21
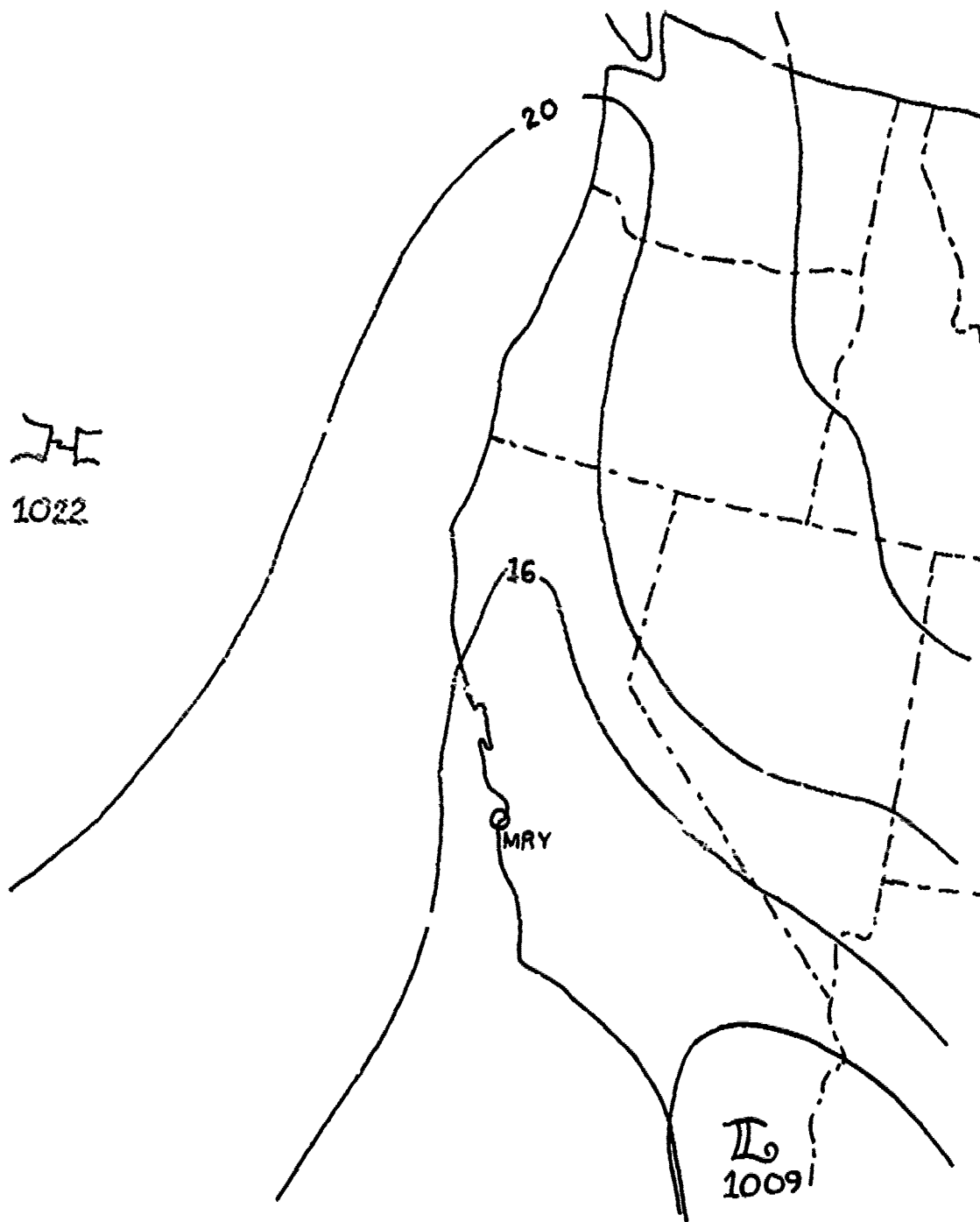
Fig. 5. Typical Surface Synoptic Pattern.
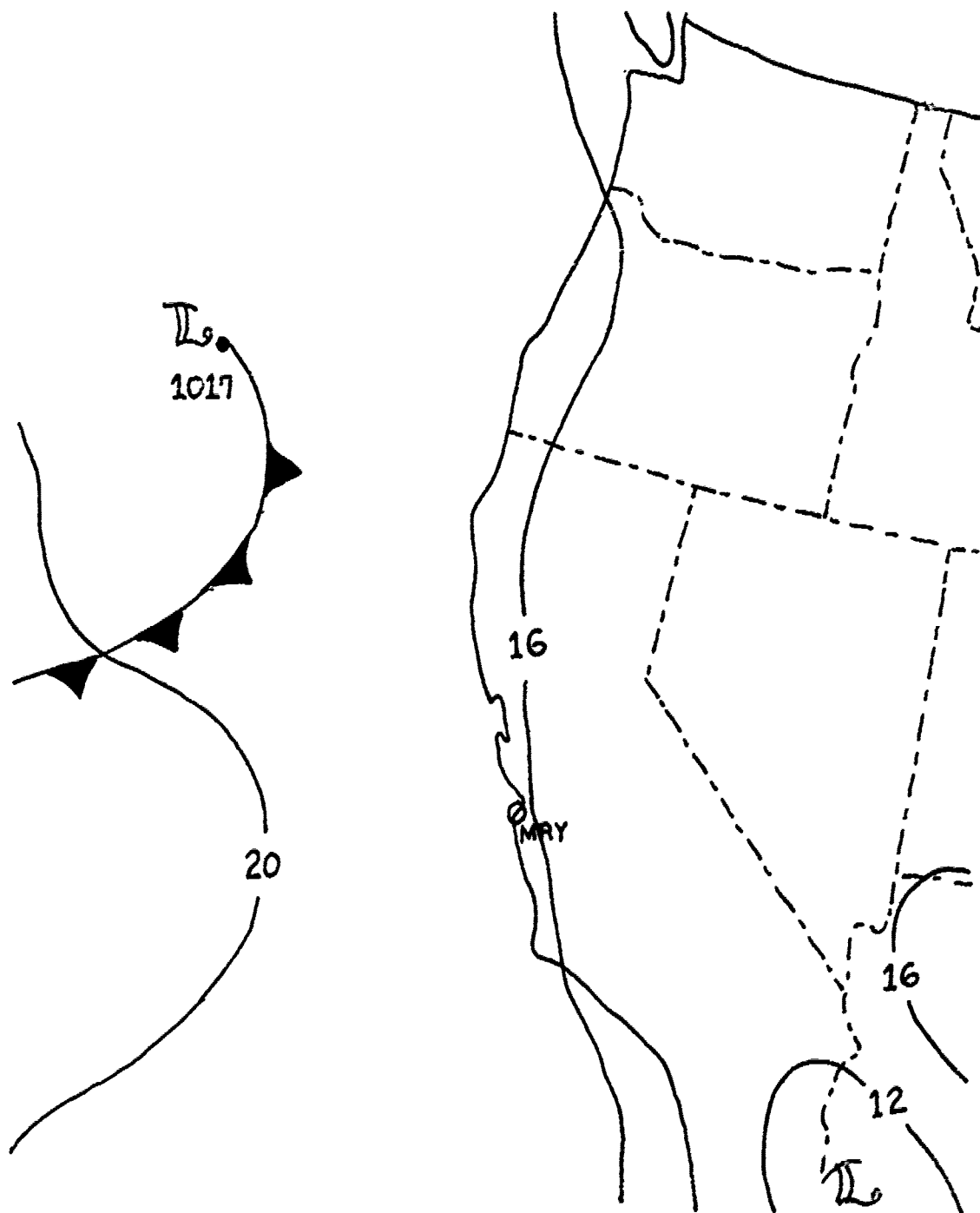
Fig. 6. Surface Synoptic Pattern: Surface pressure analysis for
         24 September, 1987.

III. PROPAGATION VELOCITY OF THE SEA BREEZE FRONT

This chapter describes the use of very simple linear geometry to determine the speed and direction of propagation of the sea breeze front. The sea breeze front was assumed to be linear within the region of the triangle created by Moss Landing Marine Laboratory, Marina Beach station and the sodar triangle. Combining this assumption with the knowledge of frontal passage times for at least three arbitrarily but precisely located surface observation stations permits the use of the method of least squares in the calculations of the speed and direction of propagation of the sea breeze front. Fig. 7 illustrates the geometry used in the frontal velocity calculations.
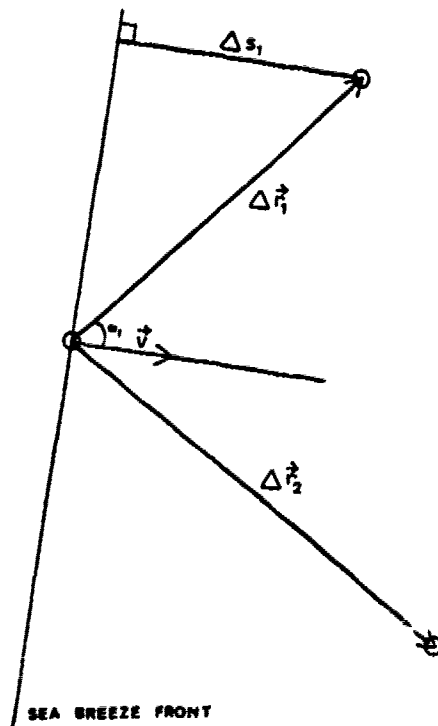
Fig. 7. Geometry for Frontal Speed and Direction of Propagation.

A. METHOD OF VELOCITY CALCULATIONS

1. Linear Front Geometry

From Fig. 7 the difference in the time of frontal passage, ,
between any two stations is

$$\Delta t_i = \frac{\Delta s_i}{\left| \vec{V} \right|} \qquad (3.1)$$

and the perpendicular distance the front travels, Δs, is

$$\Delta s_i = \left| \Delta \vec{r}_i \right| \cos \alpha_i \qquad (3.2)$$

where $\Delta \vec{r}_i$, is the spatial separation vector between the 2 stations.
Further,

$$\cos \alpha_i = \frac{\vec{V} \cdot \Delta \vec{r}_i}{\left| \vec{V} \right| \left| \Delta \vec{r}_i \right|} . \qquad (3.3)$$

Substituting equation (3.3) into equation (3.2) yields

$$\Delta s_i = \frac{\vec{V} \cdot \Delta \vec{r}_i}{\left| \vec{V} \right|} \qquad (3.4)$$

and substituting this result back into equation (3.1) gives

$$\Delta t_i = \frac{\Delta s_i}{\left| \vec{V} \right|} = \frac{\vec{V} \cdot \Delta \vec{r}_i}{\left| \vec{V} \right|^2} . \qquad (3.5)$$

Equation (3.5) can be rewritten as

$$\Delta t_i = \frac{V_x}{\left| \vec{V} \right|^2} \Delta r_{i,x} + \frac{V_y}{\left| \vec{V} \right|^2} \Delta r_{i,y} \qquad (3.6)$$

which is of the form z = mx + by.

B. LEAST SQUARES TECHNIQUE

The method of least squares is a technique which finds a "best fit"
model which comes closest to the observed data by minimizing the sum of
the square deviations between the observed and modelled values. Taking
$\frac{\partial}{\partial m}$ and $\frac{\partial}{\partial b}$ of $\sum_{i=1}^{n} (z-z_i)^2$ and setting these equal to zero minimizes

25

the sum of the squared deviations $\sum_{i=1}^{n}(z-z_i)^2$ with respect to m and b.

$$\frac{\partial}{\partial m}\sum_i [z_i - (mx_i + by_i)]^2 = 0 \tag{3.7}$$

$$\frac{\partial}{\partial b}\sum_i [z_i - (mx_i + by_i)]^2 = 0 \tag{3.8}$$

Solving equations (3.7) and (3.8) for m and b yields equation (3.9)

$$m = \frac{\sum_{i=1}^{n}y_i^2\sum_{i=1}^{n}x_iz_i - \sum_{i=1}^{n}y_iz_i\sum_{i=1}^{n}x_iy_i}{\sum_{i=1}^{n}x_i^2\sum_{i=1}^{n}y_i^2 - (\sum_{i=1}^{n}x_iy_i)^2} \tag{3.9}$$

and equation (3.10)

$$b = \frac{\sum_{i=1}^{n}x_i^2\sum_{i=1}^{n}y_iz_i - \sum_{i=1}^{n}x_iz_i\sum_{i=1}^{n}x_iy_i}{\sum_{i=1}^{n}x_i^2\sum_{i=1}^{n}y_i^2 - (\sum_{i=1}^{n}x_iy_i)^2}. \tag{3.10}$$

If we set

$$z_i = \Delta t_i,$$

$$x_i = \Delta r_{ix},$$

$$y_i = \Delta r_{iy},$$

This yields

$$m = \frac{V_x}{|\vec{V}|^2},$$

$$b = \frac{V_y}{|\vec{V}|^2}.$$

The speed of propagation of the front, $|\vec{V}|$, may be obtained by

$$m^2 + b^2 = \frac{V_x^2}{|\vec{V}|^4} + \frac{V_y^2}{|\vec{V}|^4} = |\vec{V}|^{-2}$$

or, rearranging

$$|\vec{V}|^{-1} = \sqrt{(m^2 + b^2)}. \tag{3.11}$$

The direction of propagation, Θ, clockwise from north is given by

$$\Theta = -[\tan^{-1}(\frac{V_y}{V_x})] + 90$$

or

$$\Theta = -[\tan^{-1}(\frac{b}{m})] + 90. \tag{3.12}$$

Δt, Δx and Δy can be established by taking differences between one station and any of the other stations. The reference station for this work is MLML. The precision of the experiment can be indicated by the distribution of the standard deviations of speed and direction. The standard deviation, σ, is the root mean square (rms) deviation of individual measu. ements about the universe average if were possible to make all measurements contained in the universe (Beers 1957). In this study the following derivation of the standard deviation of the measurements was employed in order to add error bars to the speed and direction of propagation results. Taking $\frac{\partial}{\partial z_i}$ of equation (3.9) yields

$$\frac{\partial m}{\partial z_i} = \frac{x_i \sum y_n^2 - y_i \sum x y_n}{\sum x_n^2 \sum y_n^2 - (\sum x_n y_n)^2}. \tag{3.13}$$

The variance of m, σ_m^2, is given by equation (3.14).

$$\sigma_m^2 = \sigma_z^2 \sum_{i=1}^{n} \left(\frac{\partial m}{\partial z_i} \right)^2$$

(3.14)

Substituting equation (3.13) into equation (3.14) gives

$$\sigma_m^2 = \frac{\sigma_z^2}{\left(\sum x_n^2 \sum y_n^2 - \left(\sum x_n y_n \right)^2 \right)^2} \sum y_n^2 \left[\sum x_n^2 \sum y_n^2 - \left(\sum x_n y_n \right)^2 \right].$$

(3.15)

Therefore, the standard deviation, σ_m, is simply the square root of the variance,

$$\sigma_m = \sigma_z \sqrt{ \frac{\sum y_n^2}{\sum x_n^2 \sum y_n^2 - \left(\sum x_n y_n \right)^2} },$$

(3.16)

with

$$\sigma_z = \sqrt{ \frac{\sum z_n^2 - 2m \sum x_n z_n - 2b \sum y_n z_n + m^2 \sum x_n^2 + 2mb \sum x_n y_n + b^2 \sum y_n^2}{k-2} }.$$

(3.17)

Similarly,

$$\sigma_b = \sigma_z \sqrt{ \frac{\sum x_n^2}{\sum x_n^2 \sum y_n^2 - \left(\sum x_n y_n \right)^2} }.$$

(3.18)

The standard deviations just calculated are used to calculate error bars for the speed and direction of frontal propagation. The precision of the speed of advance of the sea breeze front is

$$\sigma_{\vec{V}} = \left(\sqrt{(m \sigma_m)^2 + (b \sigma_b)^2} \right) |\vec{V}|^3$$

(3.19)

28

and the standard deviation of the direction of frontal propagation is

$$\sigma_\Theta = (\sqrt{(m\sigma_m)^2 + (b\sigma_b)^2})(|\vec{V}|^2). \qquad (3.20)$$

1. Determination of Time of Passage

The passage of the sea breeze front is typically marked by a sharp change in wind direction, an increase in wind speed, an increase in humidity and a decrease in temperature. The surface meteorological records of the observing stations located within the region including Moss Landing Marine Laboratory, Marine Beach, and the sodar triangle were examined for a change in wind direction toward onshore, which was considered to be $270^\circ \pm 60^\circ$. Along with the change in wind direction, changes in wind speed, temperature and humidity previously described were used to establish the time of passage of the sea breeze front. Fig. 8 illustrates a typical LASBEX surface record with the time of sea breeze frontal passage indicated by the arrow.

As was observed by Fosberg and Schroeder (1966), Schroeder et al. (1967) and Atkinson (1981), not all frontal passages are marked by a sharp change in the wind direction. For example, if the surface flow is onshore prior to the establishment of the sea breeze circulation, the passage of the front would occur without a change in this wind direction. In this situation, the discontinuities in wind speed, humidity and temperature are used for determining the passage of the sea breeze front. Fig. 9 is a surface record in which the sea breeze front passed without a sharp change in wind direction. The arrow indicates the placement of the time of passage of the sea breeze front. Table 3 lists the times of sea breeze frontal passage observed during LASBEX.

29

Table 3. TIME OF SEA BREEZE FRONT PASSAGE: Passage times are based on surface data records. Times are in decimal hours and PST.

Date	Moss Landing Marine Laboratory	Lidar	Marina Beach	Sodar 1	Sodar 2	Sodar 3
15	8.7903		8.6152	9.5001	9.5334	9.5168
16	8.9570		9.7164	10.0001	10.3834	10.2001
18	9.4570	9.479		9.8334	9.9668	9.8834
19	6.3737			7.8001	8.0501	8.0001
20	8.2070	8.440	8.6975	8.9001	9.3834	9.0001
21	8.7070	8.884	9.0854		9.7501	9.5834
22	8.7070		8.6399	9.8834	10.0001	9.9334
23	7.2903	8.118		8.7000	9.1334	9.1167
24	8.0403	8.906	9.0232	9.0501	9.3334	9.2334
26	9.7903	9.856	10.0453	10.4167	10.5001	10.4668
29	8.2903	8.499	9.1387	9.9668		9.9834
30	8.2070	8.510		9.7001		9.8334

2. Time and Distance Differences

The difference in time of passage of the sea breeze front, Δt, was determined by taking the difference between the time of frontal passage at the stations.

$$\Delta t_n = t_n - t_0$$

where t_c is the time of frontal passage at Moss Landing Marine Laboratory and t_n is the time of frontal passage at any of the other observation stations. If Moss Landing's surface data was missing, then one of the other stations would become the reference station for that day.

The same procedure just described was employed in the determination of the distances Δr_x and Δr_y.

$$\Delta r_{nx} = x_n - x_0$$
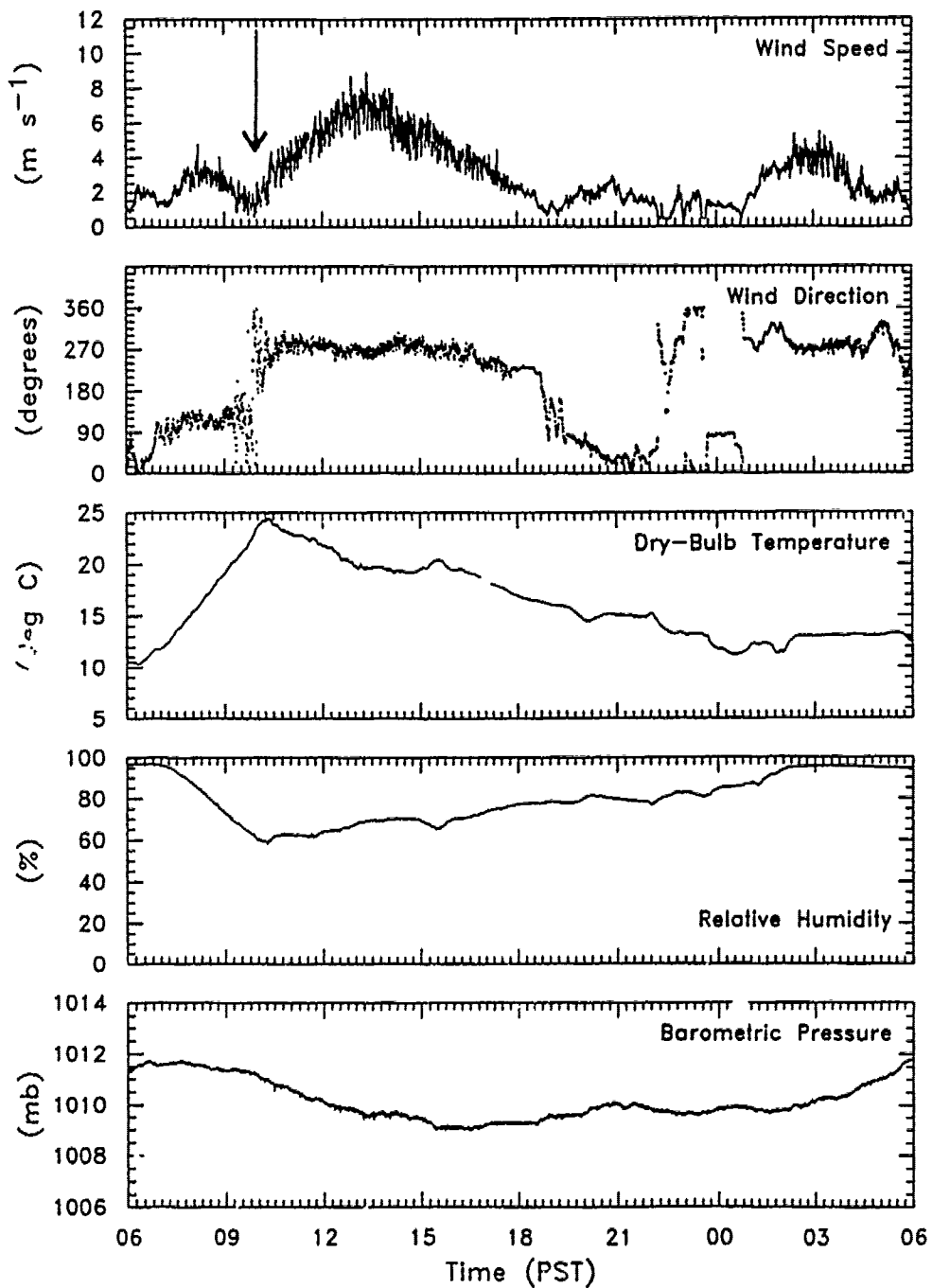
$$\Delta r_{ny} = y_n - y_0$$

Fig. 8. Surface Data Record from 16 September, 1987 at Sodar 1: Time of sea breeze front passage is indicated by the arrow.
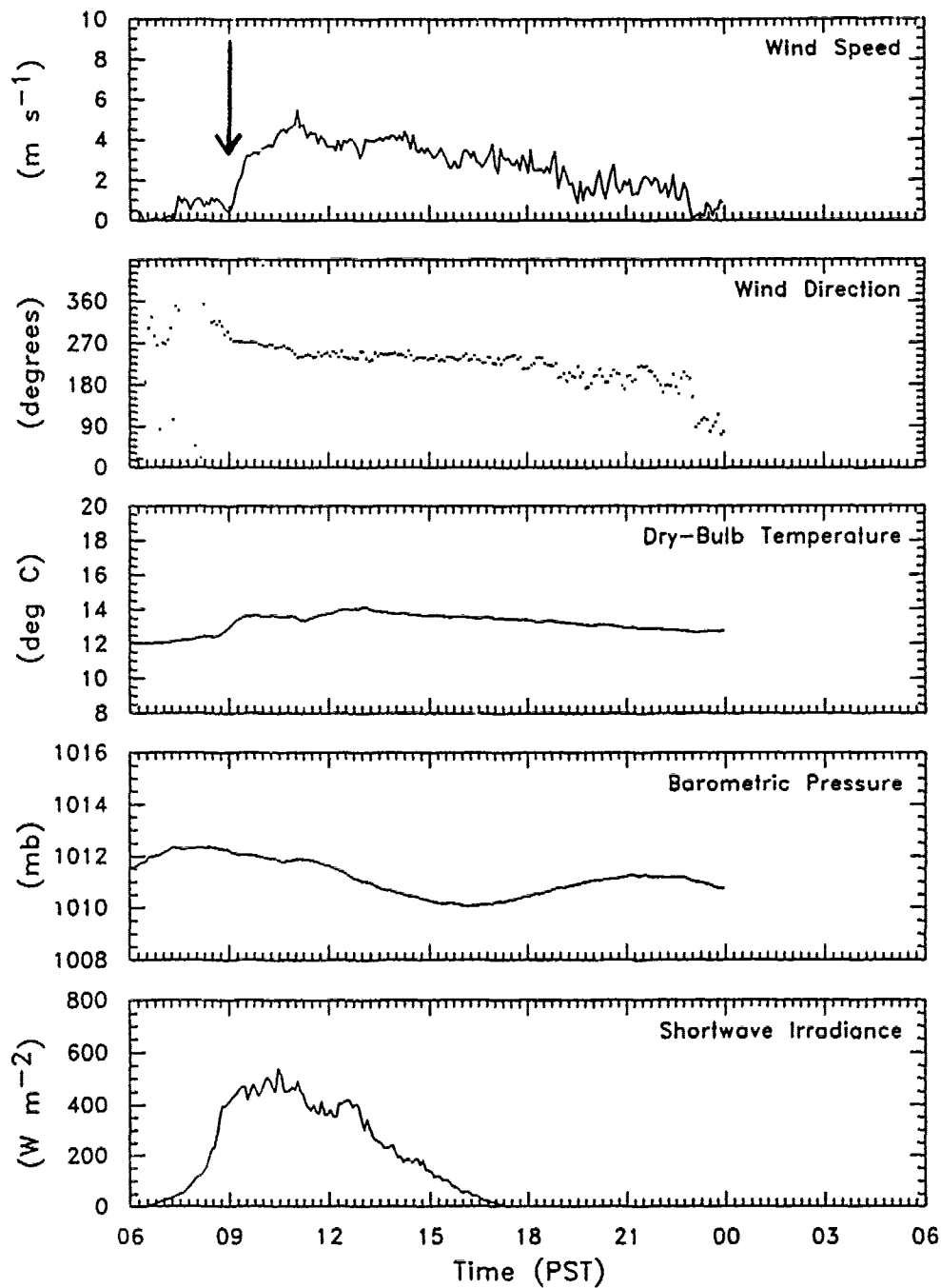
Fig. 9. Surface Record Data from 30 September, 1987 at Moss Landing Marine Laboratory: Time of sea breeze front passage is indicated by the arrow.

Table 4 lists the station coordinates which were used in the determination of the $\Delta r's$. These results were substituted into equations (3.7) and (3.8) which allow for the determination of the speed and direction of propagation of the sea breeze front.

Table 4. STATION POSITIONS: Coordinates are relative to Moss Landing
Marine Laboratory.

Station Id	East (km)	North (km)
Moss Landing Marine Laboratory	0.00	0.00
Marina Beach Station	-2.03	-12.16
Lidar	1.06	-1.10
SODAR #1	5.28	-4.64
SODAR #2	6.25	-5.61
SODAR #3	4.37	-5.93
Fritzsche Field	2.46	-13.30
Monterey Airport	-5.57	-23.40
Salinas Airport	16.63	-15.50
Monterey Bay Aquarium	-9.25	-21.75

C. RESULTS

The method of least squares yielded the results shown in Table 5. Fig. 10 which is a histogram of the speed of propagation of the sea breeze fronts observed during LASBEX shows the variability of the speed of propagation of the sea breeze front. The speed of advance of the sea breeze front ranged from 1 m/s to almost 3 m/s with a mean speed of a′ .ce of about 2 m/s ± .54 m/s. This value does not agree with t ⸝ᵑ 7 m/s speed of advance observed by Fosberg and Schroeder (1966) which was made later in the day and Olsson et al. (1973). The high frontal propagation rate observed during the afternoon by Fosberg and Schroeder (1966) was a result of the sea breeze flow being superimposed over the valley flow. The result of which is an increase in the speed of frontal propagation. Olsson et al. (1973) observed propagation

speeds of 5 to 7 m/s in a corridor situated between the coastal ranges which parallel Oregon's coast. The net effect of the mountain and natural gap orientation is to create a funneling effect. This results in increased propagation speeds of the sea breeze front. However, a 2 m/s speed of advance of the sea breeze front is in good agreement with the 2 to 3 m/s results reported by Simpson et al. (1977) and summarized by Atkinson (1981).

Table 5. FRONTAL SPEED AND DIRECTION OF PROPAGATION

Date	Speed (m/s)	Direction (deg)
15	2.19 +/- .14	93.6 +/- 5.8
16	1.65 +/- .13	121.7 +/- 4.0
18	2.52 +/- .76	133.3 +/- 36.7
19	1.20 +/- .16	161.6 +/- 3.6
20	2.22 +/- .16	118.1 +/- 6.7
21	1.78 +/- .18	105.4 +/- 6.0
22	1.38 +/- .19	98.5 +/- 5.0
23	1.28 +/- .75	184.9 +/- 18.4
24	1.74 +/- .39	130.3 +/- 12.9
26	2.91 +/- .17	112.7 +/- 4.1
29	1.67 +/- .16	104.9 +/- 5.0
30	2.42 +/- .36	134.8 +/- 16.6

Fig. 11 is a histogram of the direction of propagation of the sea breeze fronts observed during LASBEX. The mean direction of sea breeze frontal propagation was east to southeast at $125^\circ \pm 26^\circ$. For a straight, level coastline the theoretical propagation direction of the sea breeze front would be eastward. The propagation direction of 125° implies a tendency for the sea breeze to propagate down the Salinas Valley, which is orientated at roughly 140°. This observation is in good agreement with observations made by Fosberg and Schroeder (1966), Schroeder et al. (1967), Olsson et al. (1973) and Johnson and O'Brien (1973) that the penetration of

the marine air inland is through natural gaps and passages in the coastal mountain ranges. The propagation direction of 180° occurred on a day in which the sea breeze front was "poorly defined". This could result in a decrease in the accuracy of determination of the time of frontal passage time.
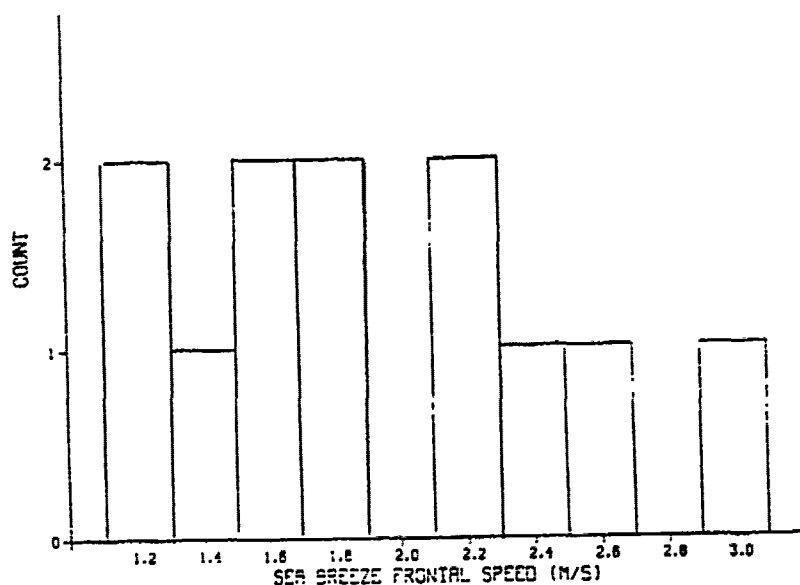
Fig. 10. Histogram of Sea Breeze Frontal Speeds.
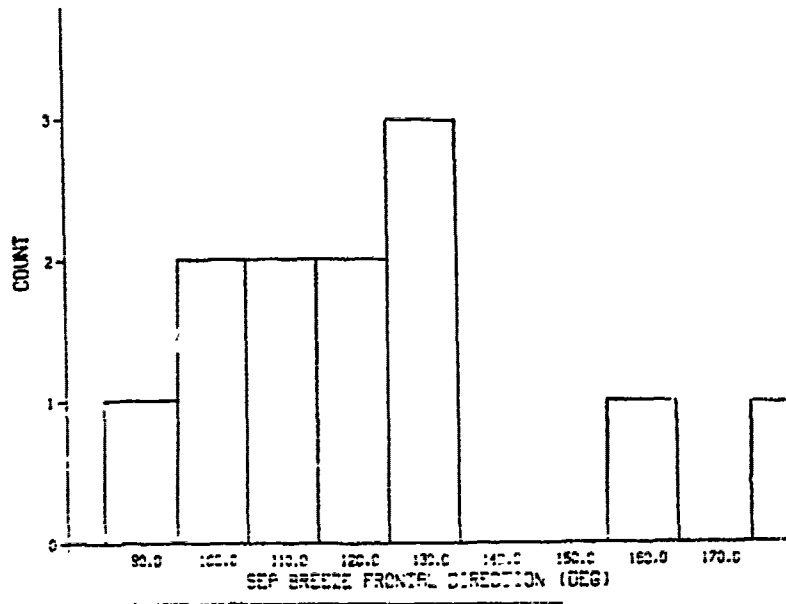
Fig. 11. Histogram of Sea Breeze Direction of Propagation.

IV. SURFACE HEAT FLUX

A. WELL MIXED BOUNDARY LAYER

The thermodynamic condition of stable stratification over the cool ocean and convective mixing over the heated land are important to the development of a sea breeze flow (Simpson et al. 1977). The inland movement of the sea breeze can vary significantly due to changes in differential heating. An analogy to a heat engine might be appropriate at this point. The more fuel (differential heating) added to the engine the faster the engine will operate and the greater speed of frontal propagation. This chapter will describe a means to estimate the surface heat flux, $\overline{w'\theta'}_s$, for comparison to the speed of propagation of the sea breeze front.

B. METHOD OF SURFACE HEAT FLUX CALCULATION

1. The Well Mixed Boundary Layer

Under conditions of free convection the boundary layer is considered to be well mixed between the earth's surface and the mean height of the inversion. Therefore, potential temperature and specific humidity are constant with height above the surface layer. At the inversion interface, the downward entrainment of warm air implies a downward or negative heat flux. The heat flux goes to zero as turbulence disappears in the inversion. Entrainment at the inversion and solar heating at the earth's surface combine to warm the mixed layer. Because the layer is well-mixed, the heat flux profile is linear between the negative values at the inversion base and the positive values at the

37

earth's surface (Stull 1976). Fig. 12 illustrates the idealized
boundary layer heat flux profile which was just described.

The height of the boundary layer is the height at which the
stable stratified inversion layer extinguishes the turbulence found in
the boundary layer (Stull 1976). The boundary layer height, h, may
range from the surface to more than 3 km in conditions of large static
stability and conditions of free convection respectively (Huschke 1986).
In the midlatitudes, the boundary layer extends through the lowest
1 km of the atmosphere.

2. Surface Heat Flux Calculation

Heat balance is the equilibrium which exists when all sources
of heat gain and loss for a given region are accounted for. In general,
this balance, which results from the first law of thermodynamics,
includes advection as well as a radiative term (Huschke 1986).

$$\frac{\partial \bar{\theta}}{\partial t} + \vec{V} \cdot \nabla_H \bar{\theta} + \frac{\partial R}{\partial z} + \frac{\partial \overline{w'\theta'}}{\partial z} = 0 \qquad (4.1)$$

Prior to the passage of the sea breeze front the winds are
light and variable and advection may be neglected. Additionally,
radiative heating of the atmosphere is neglected in this study. With
these assumptions, equation (4.1) reduces to equation (4.2).

$$\frac{\partial \bar{\theta}}{\partial t} + \frac{\partial \overline{w'\theta'}}{\partial z} = 0. \qquad (4.2)$$

As previously mentioned, the heat flux profile in a convection boundary
layer is linear and subsequently the variation of the heat flux, $\overline{w'\theta'}$,
with height can be replaced with the difference between the extreme
values of heat flux over the boundary layer height. This yields
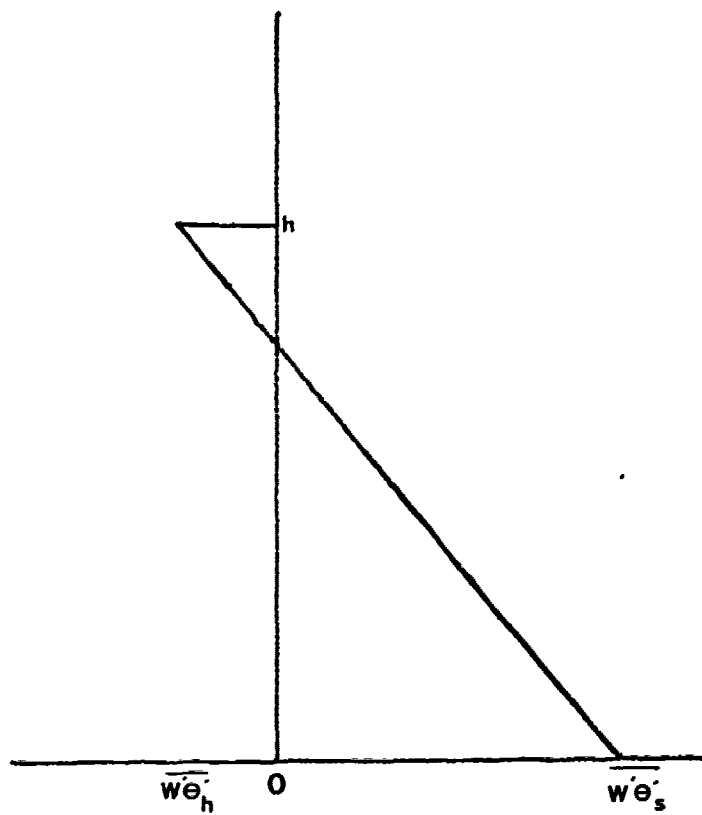equation (4.3).

Fig. 12. Idealized Heat Flux Profile: This profile is for a well mixed boundary layer.

$$\frac{\partial \bar{\theta}}{\partial t} = -\frac{\partial \overline{w'\theta'}}{\partial z} \approx \frac{\overline{w'\theta'}_s - \overline{w'\theta'}_h}{h} \tag{4.3}$$

Under free convection conditions, the friction velocity, the magnitude of the wind velocity across the interface and energy loss rate due to internal gravity waves are small and the entrainment heat flux, $\overline{w'\theta'}_h$, can be approximated as a constant fraction of the surface heat flux, $\overline{w'\theta'}_s$ (Stull 1976).

$$-(\overline{w'\theta'})_h = A_1 (\overline{w'\theta'})_s \tag{4.4}$$

The constant fraction, A_1 ranges from 0.1 to 0.3. Table 6 lists both experimentally observed and theoretically assumed A_1 values. 0.2 was the value chosen for A_1. This yields equation (4.5).

$$\overline{w'\theta'}_h = -.2\overline{w'\theta'}_s \tag{4.5}$$

Through substitution, equations (4.3) and (4.5) combine to yield an equation which allows for the estimation of the surface heat flux, $\overline{w'\theta'}_s$ in terms of quantities which were readily observable during LASBEX. These results do not take into account any effect of clouds.

$$\overline{w'\theta'}_s \approx \frac{5h}{6}\frac{\partial\bar{\theta}}{\partial t} \tag{4.6}$$

Data to evaluate equation (4.6) are available from the primary sodar site.

3. Boundary Layer Height

Two methods were available for determining the height of the boundary layer. First, temperature and dew point temperature data from radiosonde launches were used to find the height of the inversion base

40

marking the top of the boundary layer. At the top of the boundary layer the temperature and dew point curves separate rapidly marking the transition to warmer drier air above the atmospheric boundary layer. Therefore, the sudden separation of the temperature and dew point curves can be used as an indicator of the boundary layer height. The number of radiosonde launches prior to the passage of the sea breeze front were limited, however.

The second method of boundary layer height determination employed in this study made use of the wind profile tables generated by the sodar. The vertical profiles of wind direction, wind speed and the standard deviation of the vertical velocity, σ_w, were used to determine the height of the boundary layer. A change in wind direction in conjunction with an increase in wind speed and a decrease in σ_w toward zero were the indicators of the location of the boundary layer height. Fig. 13 provides wind table profiles and radiosonde profiles for the same time period. A comparison of the profiles shows that the boundary layer height derived from the two systems is comparable. In the early morning, when the boundary layer is shallow, the sodar data would not be useful. This is due to the fact that sodar profiles start at 75 m, and the height of the boundary layer could be below this level.

4. Local Change of Temperature With Time

As long as the boundary layer is well-mixed, $\frac{\partial \bar{\theta}}{\partial t}$ is the same at all levels. This means that the change of potential temperature with time at the surface is the same as the change of potential temperature at any level in the well mixed boundary layer.

Table 6. PUBLISHED VALUES OF HEAT FLUX RATIO A_1: Values are either experimentally observed (O) or theoretically assumed (T) (after Stull 1976).

A_1	Investigator	Year	Type
0.1	Lenschow	1970	O
0.1	Deardorff	1972	O
0.15	Stull	1973	T
0.13	Deardorff	1973	T
-0.04 - 0.17	Lenschow	1973	O
0.1	Stull	1973	O
0.2	Deardorff	1973	O
0.2	Tennekes	1973	T
0 - 0.5	Carson	1973	O
0.25	Betts	1973	O
0.25	Carson	1973	T
0.5 - 2.0	Coulman	1973	O
0.12	Lenschow	1974	O
0.10	Pennell & LeMone	1974	O
0.21	Deardorff	1974	T
0.17	Deardorff	1974	T
0.20	Deardorff	1974	T
0.19	Deardorff	1974	T
0.14	Deardorff	1974	T
0.23	Stull	1974	T
0.29	Cattle & Weston	1974	O
0.32	Cattle & Weston	1974	O
0.25	Raymond & Readings	1974	O
0.23	Deardorff, Willis & Lilly	1974	OT
0.30	Betts	1974	OT
0.11 - 0.23	Willis & Deardorff	1974	O
0.2	Sarachik	1974	T
0.2 - 0.5	Tennekes & Van Ulden	1975	O

Using surface data, from the sodar 1 site, a linear regression line was found for the temperature records prior to the passage of the sea breeze front. Fig. 14 shows the surface record for 29 September, 1987 and Fig. 15 illustrates the regression line fitted to the temperature record for the same date. The slope of this line provides $\frac{\partial \bar{\theta}}{\partial t}$. Finally, equation (4.6) on page 40 yields surface heat flux estimates prior to the passage of the sea breeze front.

C. RESULTS

Table 7 lists the results of the surface heat flux calculations,
which range from about 100 W/m^2 to about 400 W/m^2. A scatter diagram,
Fig. 16, clearly shows a correlation between the surface heat flux and
the speed of frontal propagation. In general, the larger surface heat
flux values appear to result in a faster moving sea breeze front.
Although the observations were collected in the presence of clouds, the
trend observed in Fig. 16 would probably be the same if the effects of
clouds could be included in the heat flux estimation. The presence of clouds
would increase the fraction of the surface heat flux required to approximate
the entrainment heat flux, thereby altering the slope of the regression
line. Using the shortwave irradiance measured at Moss Landing Marine
Laboratories in conjunction with radiosonde data as an indicator of
cloud presence, it should be noted that on the majority of the days
during LASBEX there appears to be a stratus deck present at the mouth
of the Salinas Valley prior to the passage of the sea breeze front.

D. ADDITIONAL OBSERVATION

1. Comparison to Feliks' (1988) Results.

In Chapter 1, Feliks' (1988) investigation of the inland
penetration of the sea breeze circulation was cited. His assumption of
constant frontal speed and structure are similar to those used in this
study. Feliks' surmised that the square of the frontal speed relative
to the synoptic wind is proportional to the mean drop of potential
temperature across the frontal area multiplied by the frontal height.
The basic elements to test this are present in the LASBEX data set.
Frontal speeds were calculated in Chapter 3. Geostrophic winds were
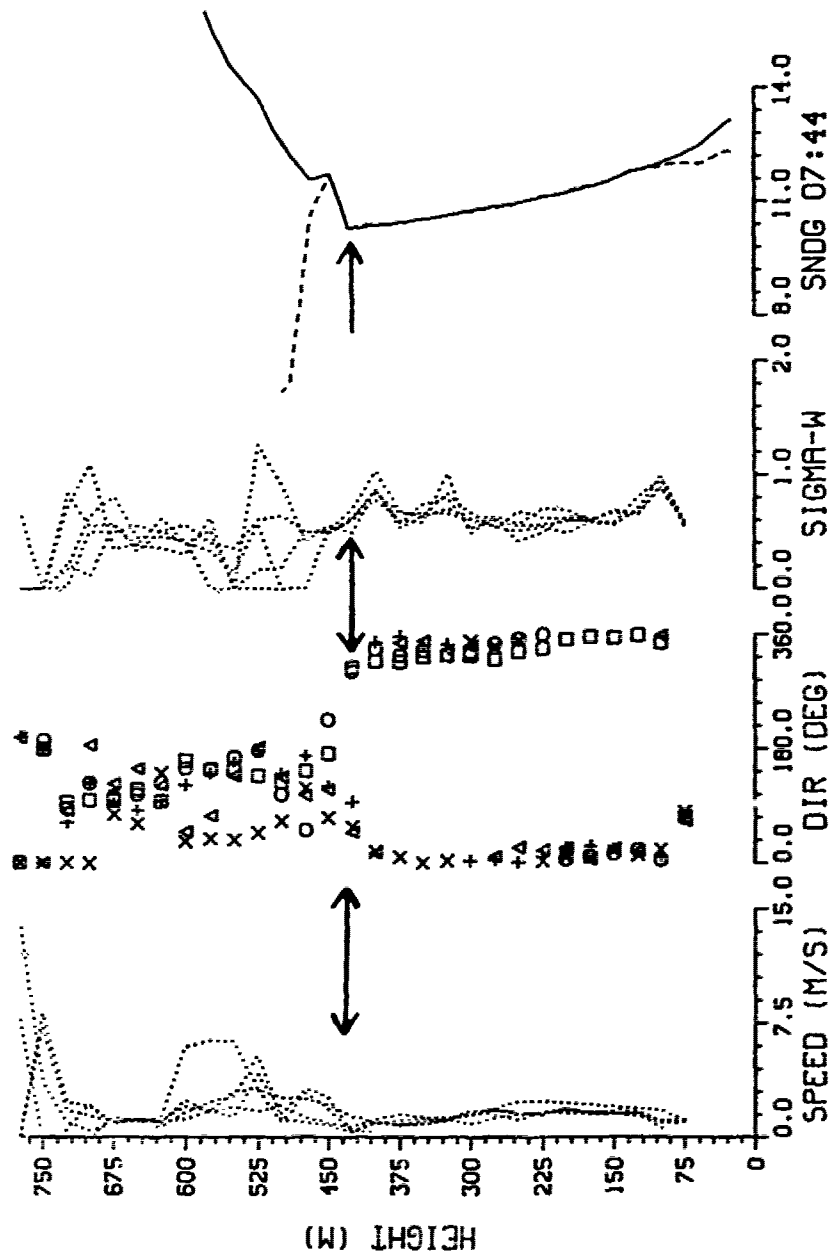
Fig. 13. Vertical Profiles from Sodar and Radiosonde for 18 September,
1987: Sodar data at 5 min intervals, 0726 to 0746 PST.
Radiosonde sounding at 0744 PST. Arrows indicate boundary
layer height.
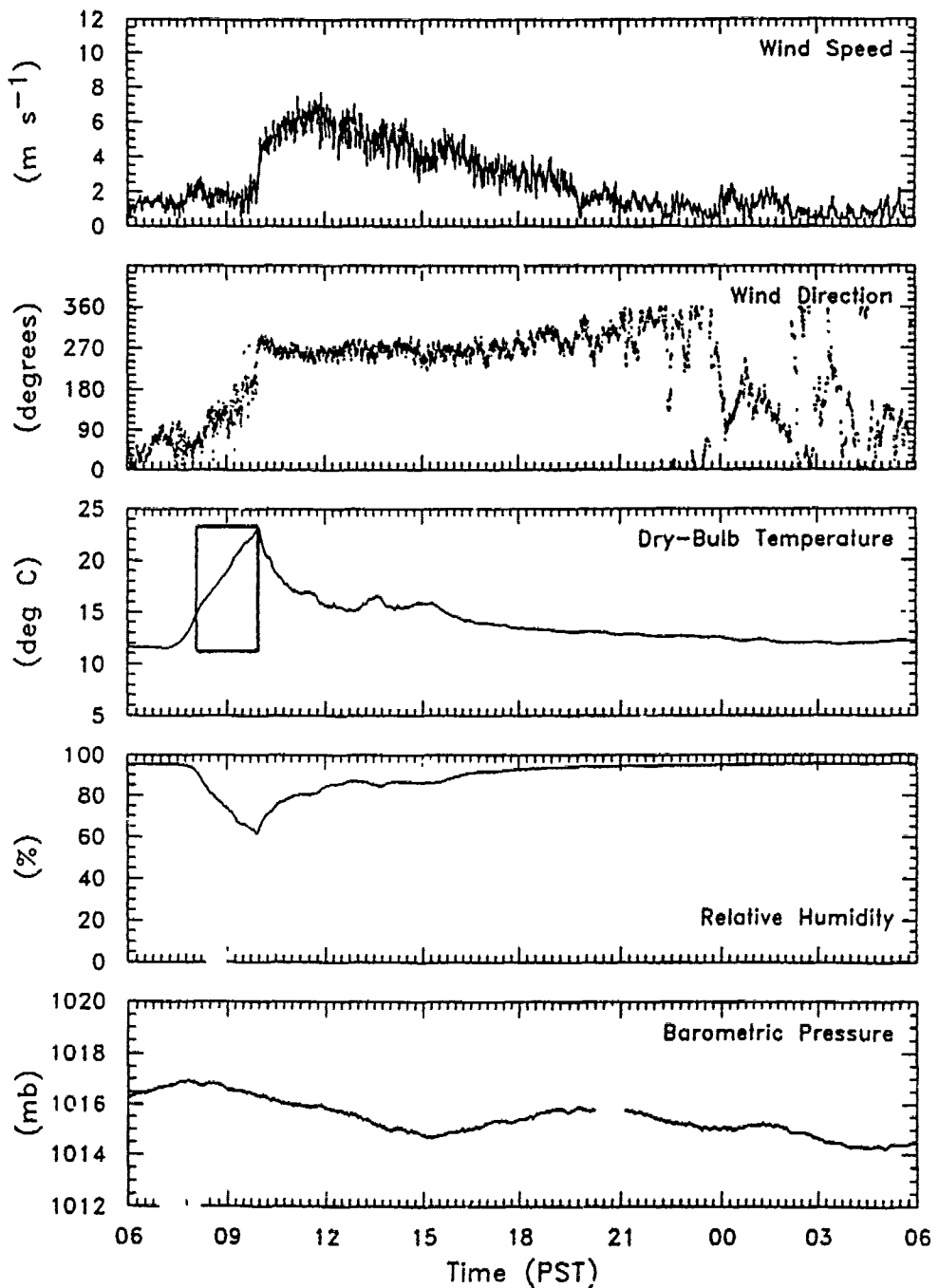
44

Fig. 14.   Surface Record From 29 September, 1987 at Sodar1:   Boxed area
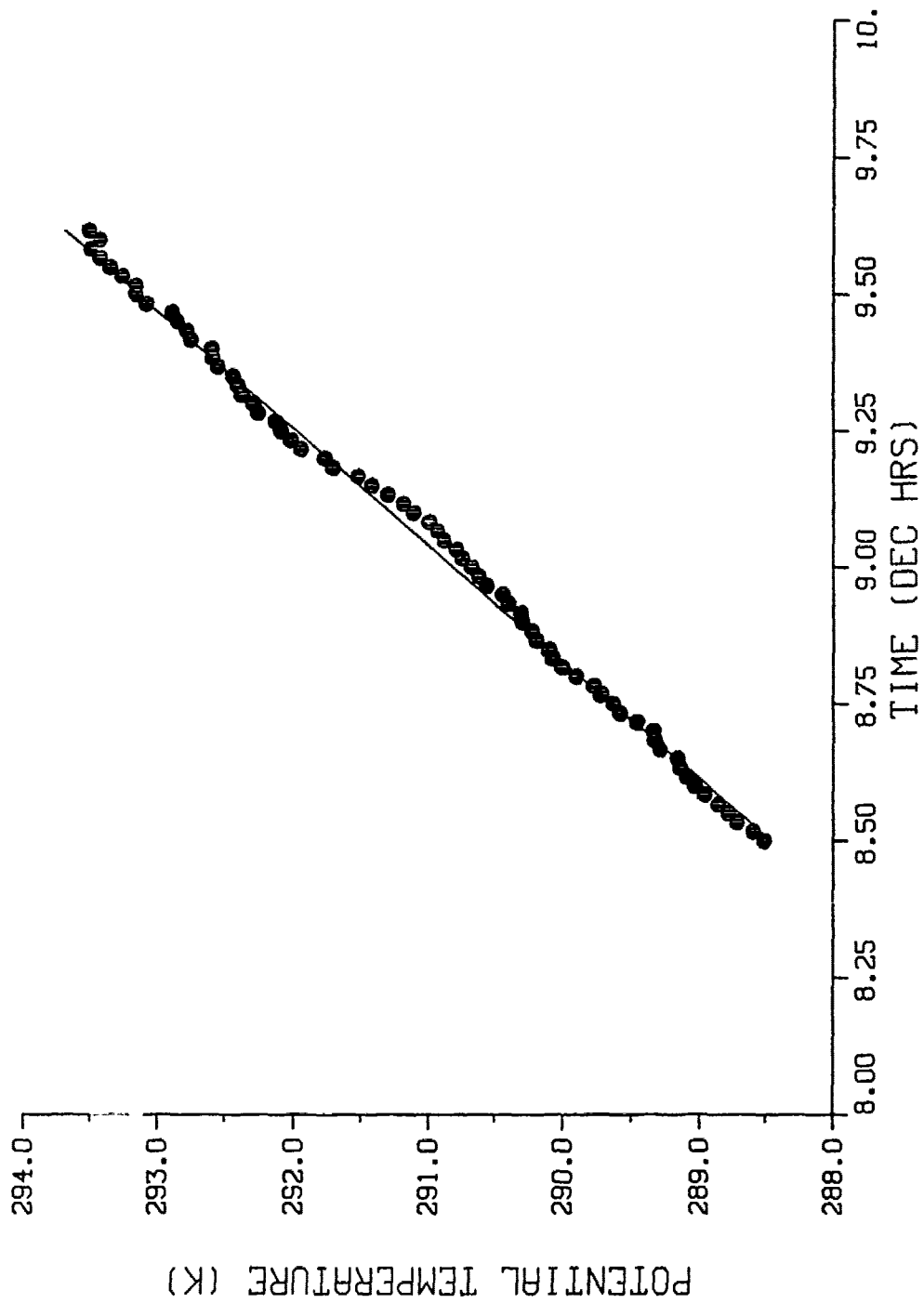   is shown in Fig. 15.

45

Fig. 15. Prefrontal Temperature Record for 29 September, 1987: The solid line is the regression line which "best fits" this data.

obtained from Oakland soundings. The geostrophic level is roughly

located at an altitude of 1 km. With the exception of a few mountain

peaks, this level is above significant topographic features. Therefore,

in addition to soundings from the R/V Silver Prince, Oakland soundings

were considered representative of the geostrophic level in the Monterey

Bay. The radius of the sea breeze front was approximated as the height

of the sea breeze front at time of passage, which was ascertained from

wind direction time height cross sections presented in Fagan (1988).

Fig. 17 is an example of the time height cross sections from which the

frontal height was determined. The surface data records allowed for

the easy determination of the change of potential temperature across

the sea breeze front. Table 8 provides a list of the data set.

Fig 18 provides a scatter diagram of the results from these

calculations. The distribution of the data points indicates that there

is a relationship between frontal speed relative to the synoptic flow

and the drop of potential temperature across the front multiplied by

the height of the sea breeze front. The extreme value is found on

23 September which was a day in which the sea breeze front was diffuse

at best. Therefore, this value might not be too representative of a

sea breeze day. In general, these results are in agreement with the

results of Feliks (1988).

Table 7. SURFACE HEAT FLUX RESULTS: Boundary layer heights were
obtained from sodar wind tables produced at the primary
sodar site.

Date	Boundary layer height (m)	$\overline{w'\theta'}_s\,(W/m^2)$
16	230	351.03
18	420	331.73
20	210	277.65
21	225	255.35
22	320	127.07
23	450	73.39
24	105	189.17
27	120	154.91
29	270	356.47
30	225	394.40
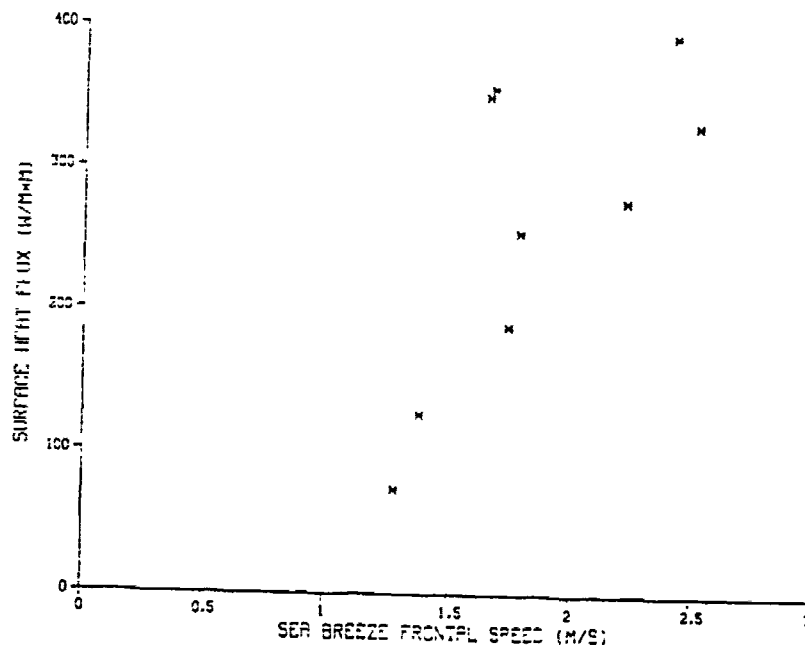
Fig. 16. Scatter Diagram. Surface heat flux versus speed of
propagation of the sea breeze front is plotted.
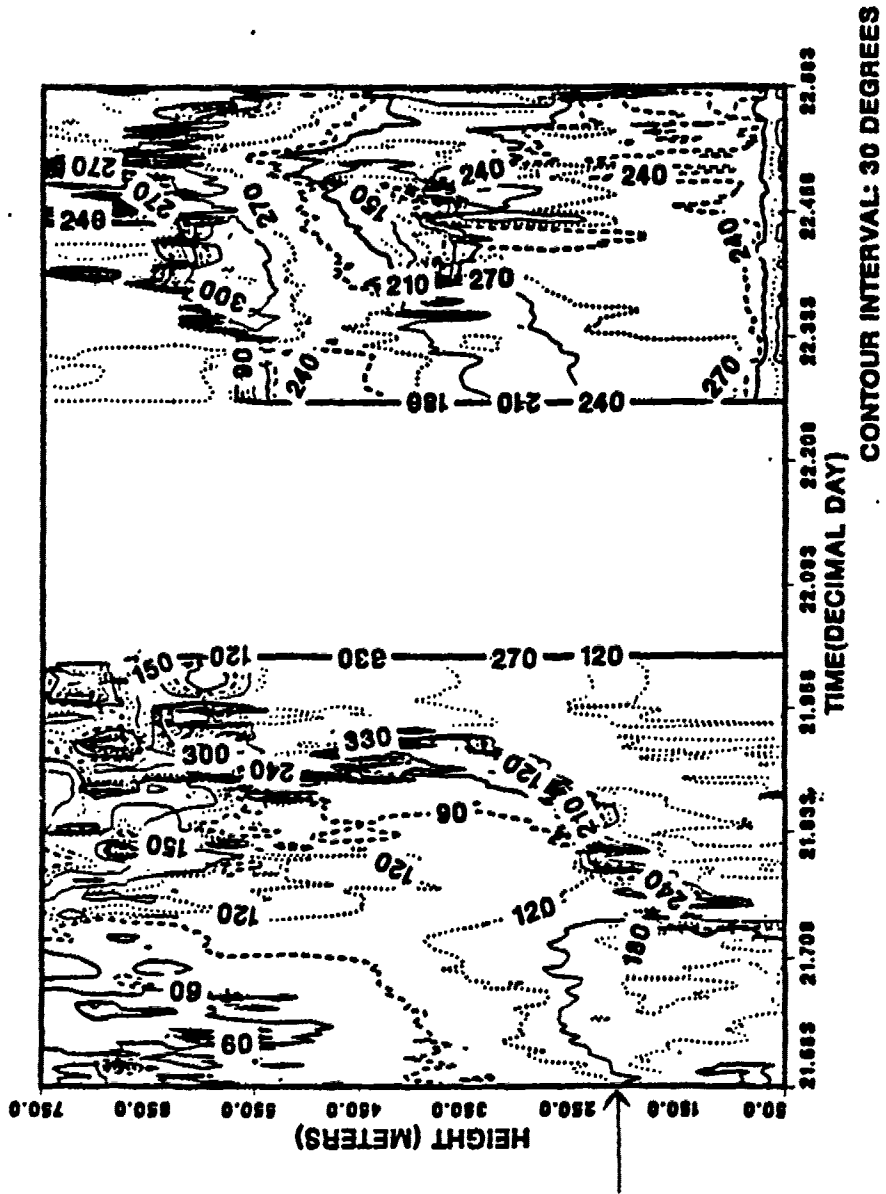
Fig. 17. Time Height Cross Section for 21 September 1987: Arrows indicate placement of frontal height. (from Fagan 1988).

49

Table 8. FRONTAL SPEED, GEOSTROPHIC FLOW, FRONTAL HEIGHT AND POTENTIAL TEMPERATURE CHANGE ACROSS THE FRONT: C = frontal speed; U = geostrophic flow; dir = U direction; h = frontal height; ΔT= drop in Θ across the front.

Date	c(m/s)	U (m/s)	Dir (°)	h (m)	ΔT(K)
16	1.65	4.63	075	175	0.6
18	2.52	3.60	240	205	0.5
19	1.20	1.36	300	130	0.3
20	2.22	3.15	170	120	0.6
21	1.78	5.14	045	130	0.9
22	1.38	7.20	320	315	0.5
23	1.28	12.49	326	400	0.4
29	1.67	5.14	175	135	0.8

Fig. 18. Scatter Diagram: $(c - U)^2$ versus ΔTh is plotted.

V. MESOSCALE CHARACTER OF FRONTAL PROPAGATION

The sea breeze front was assumed to be linear within the triangle formed by the observation stations at Moss Landing Marine Laboratory, Marina Beach and the sodar triangle. Surface time series for the stations which were located outside this triangle were examined for any indication of a sea breeze front passage. These stations regularly displayed a reco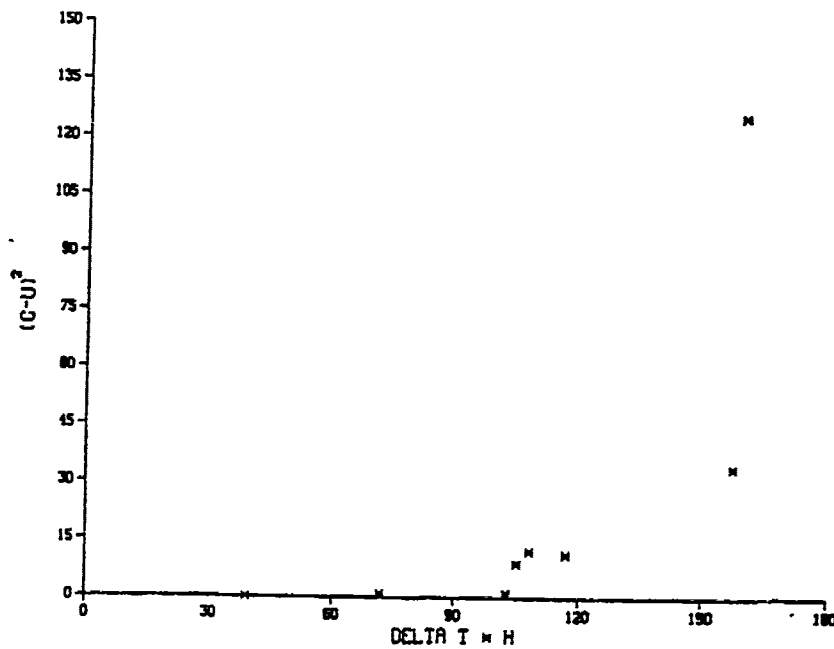gnizable sea breeze front feature in their 24 hour surface records. This chapter will explore the degree to which the front deviates from linear by comparing a linearly extrapolated frontal passage time with the observed time of frontal passage at the primary sodar site and examined the hourly wind vectors for three days, 16, 18 and 29 September, which exhibited a sharp sea breeze front.

A. LINEAR EXTRAPOLATION OF THE FRONT

The direction of propagation of the sea breeze front is perpendicular to the front. The distance between the primary sodar site and the observation stations to which the sea breeze front is being extrapolated is given by

$$D = \sqrt{(x_n - x_1)^2 + (y_n - y_1)^2}.$$ (5.1)

The station coordinates given in Table 4 are entered into equation (5.1). This gives the distance, D, between the primary sodar site and the station of interest. From Fig. 19 the angle between D and the perpendicular distance the front has traveled is

$$\phi = 90 - (\alpha + \gamma),$$ (5.2)

where

$$\alpha = \Theta - 90,$$ (5.3)

51

and

$$y = 90 - \sin^{-1}(\frac{y}{D}).$$
(5.4)

From simple trigonometry,

$$\cos \phi = \frac{d}{D}.$$
(5.5)

Rearranging,

$$D \cos \phi = d.$$
(5.6)

The time, t, required for the sea breeze front to traverse d, which is the perpendicular distance the front travels, is given by equation (5.7).

$$t = \frac{d}{r}$$
(5.7)

where r is the speed of frontal propagation calculated in Chapter 3. This result is added to the time of frontal passage at the primary sodar site. This yields an expected time of arrival of the sea breeze front if the front maintained its linear structure and maintained its speed of advance. This value can be compared to the observed arrival time of the sea breeze front at the station of interest to give an estimate of frontal acceleration, deceleration or departure from linear. For the hourly reporting stations, the observation times were moved ahead a half hour in order to reduce the maximum error in the observation time to 30 min. Fig. 19 provides a schematic of the extrapolation idea just described.

B. HODOGRAPHS OF HOURLY WIND VECTORS

Hodographs of hourly wind vectors for 16, 18, and 29 September, 1987 were generated for analysis. Figs. 19, 20, and 21 are hodographs of the hourly wind vectors at Moss Landing Marine Laboratory for 16, 18 and 29 September respectively. If the area were completely free from any local influences, the wind vectors should show a clockwise

turning with time (Fosberg and Schroeder 1966, Atkinson 1981). However, during LASBEX a counterclockwise turning of the wind was observed. Perhaps the sea breeze flow is superimposed upon the monsoonal flow which deter the offshore flow usually expected in the early morning. This is in agreement with observations made by Fosberg and Schroeder (1966) in the San Francisco Bay area. Of note is what appears to be a second inland penetration of marine air onto the central coast on 16 September. Prior to the second inland penetration of marine air, the surface flow was offshore and weak. This double penetration phenomena lends itself to future research.

C. RESULTS OF LINEAR EXTRAPOLATION

The linear extrapolation of the sea breeze front was divided into two categories based on the locations of the stations of interest relative to Moss Landing Marina Beach, and the sodar triangle. First, the stations located to the south, Monterey Bay Aquarium and the Monterey Airport, are examined. Table 9 provides the times of frontal passage, the extrapolated times of frontal passage and the difference between the two times of passage. Both Monterey Bay Aquarium and Monterey Airport exhibit large differences between the extrapolated and observed times of sea breeze frontal passage. At the Monterey Bay Aquarium, the frontal passage time difference, Δt, ranged from -1.66 decimal hours to 1.17 decimal hours. The negative sign indicates that the observed time of frontal passage was later than the extrapolated time of frontal passage. At the Monterey Airport, Δt varied from -.91 decimal hours to 1.42 decimal hours. The large deviations are probably a result of the local topography altering the shape of the sea breeze

53
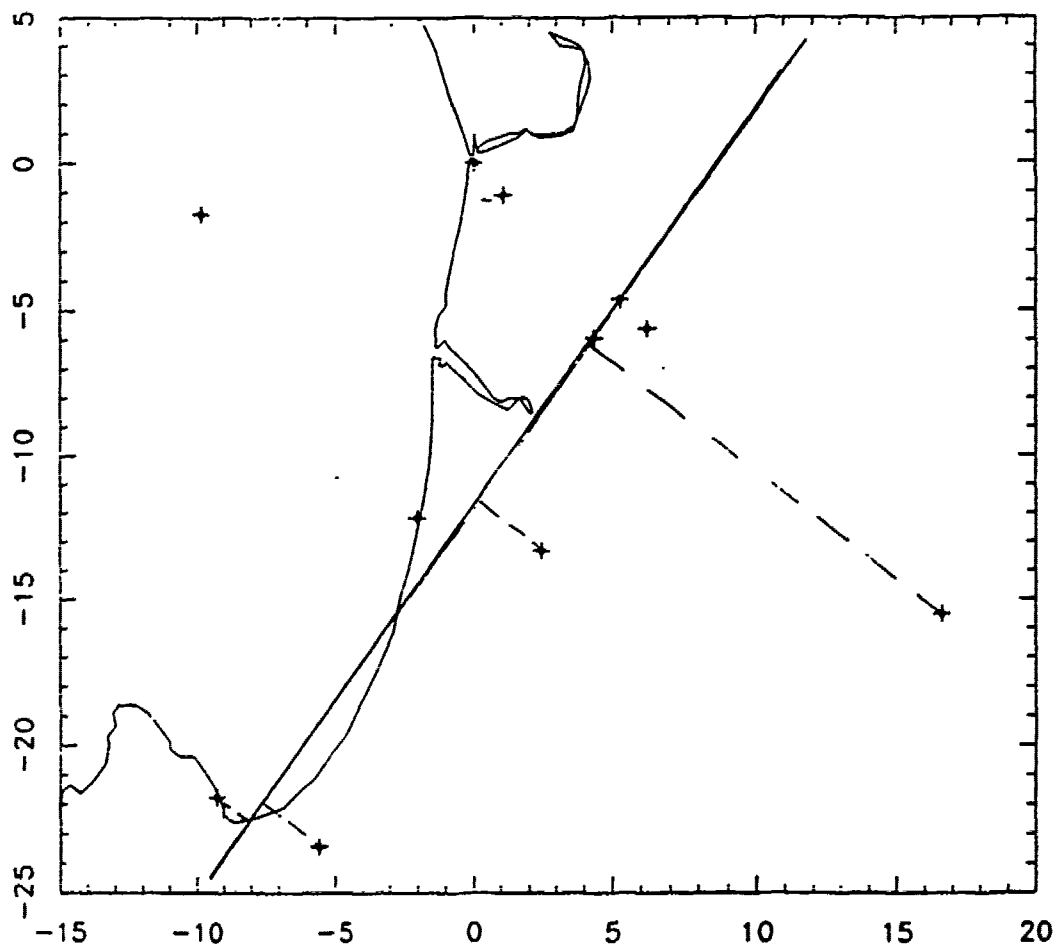
Fig. 19. Schematic of Linear Extrapolation of the Sea Breeze Front:
The solid line is the linear front. The dashed lines represent
the extrapolation of the front to the other stations.
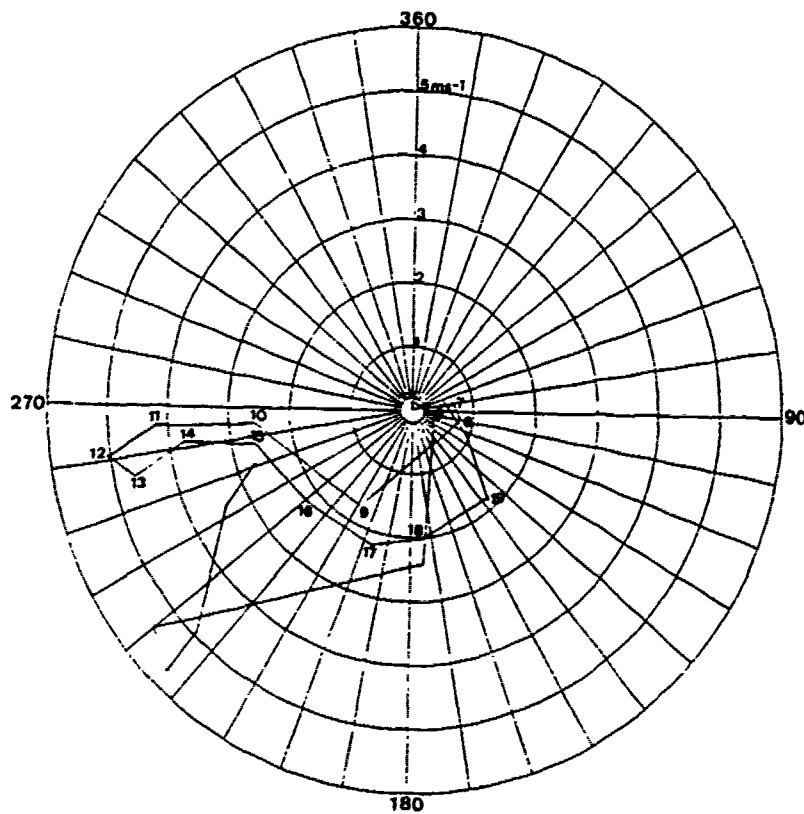
Fig. 20. Hodograph of Hourly Wind Vectors at Moss Landing for 16
September, 1987: Times are PST and are labelled from
0600 to 1900.
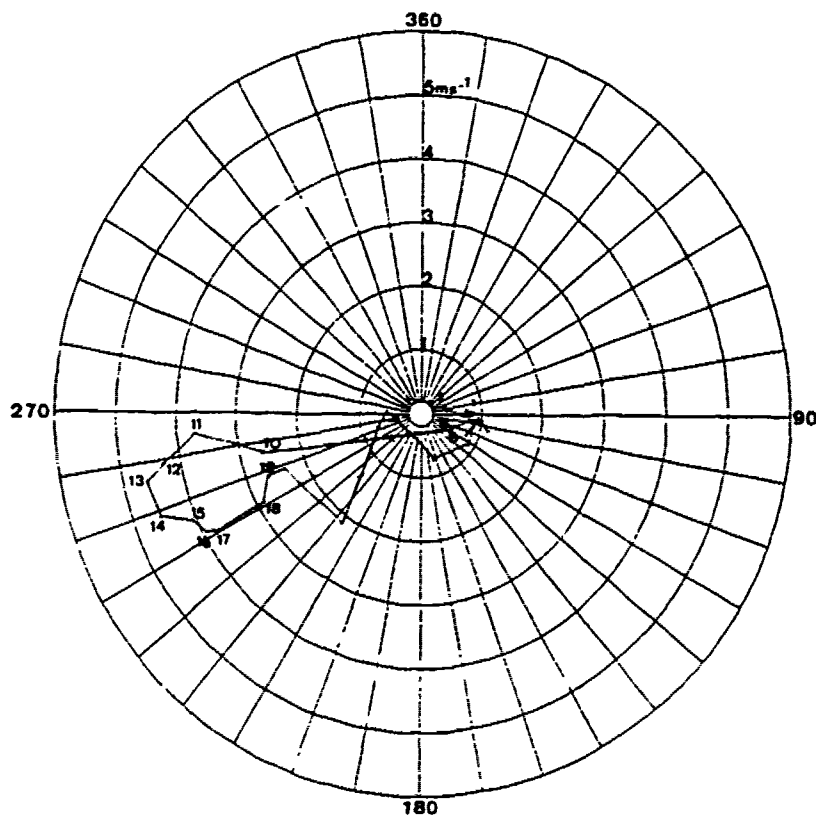
Fig. 21. Hodograph of Hourly Wind Vectors at Moss Landing for 18
September, 1987: Times are PST and are labelled from
0600 to 1900.
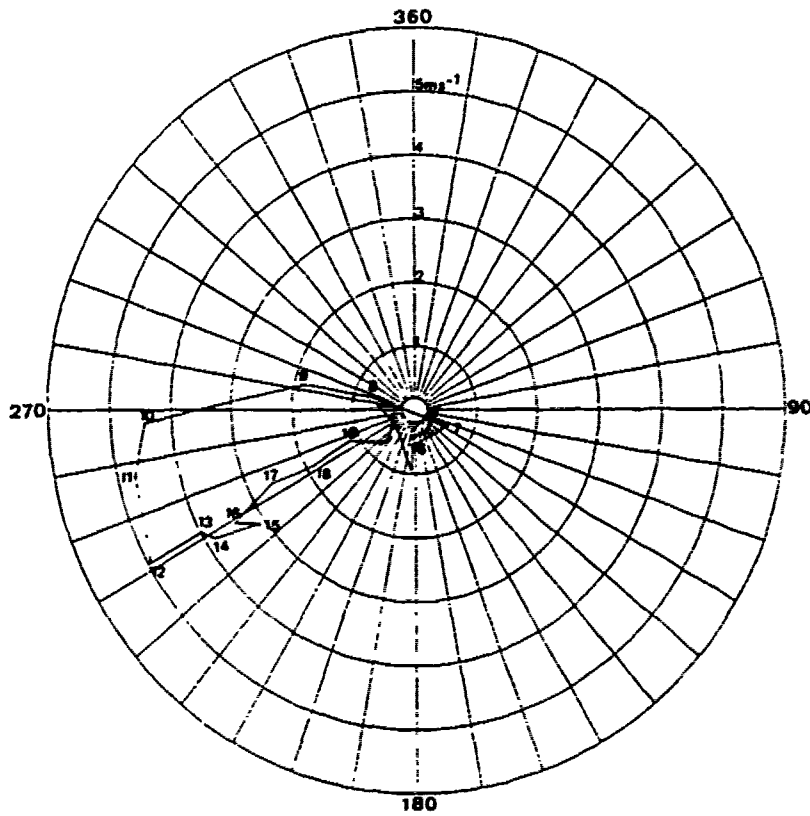
Fig. 22. Hodograph of Hourly Wind Vectors at Moss Landing for 29
September, 1987: Times are PST and are labelled from
0600 to 1900.

front. This indicates that in the southern portion of Monterey Bay the sea breeze front is curved.

Next, the stations to the east, Fritzsche Field and Salinas Airport were examined. Table 10 provides the observed frontal passage times, the extrapolated frontal passage times and the difference between the two passage times. Differences in arrival times at Fritzsche Field ranged -.14 to .26 decimal hours. Since Fritzsche Field was much closer to the initial observation stations, the difference between the arrival times is much less than those observed at Monterey Bay Aquarium and Monterey Airport. The differences in the arrival times at Salinas Airport ranged from -.66 to 1.31 decimal hours. Once again, large variability in Δt is observed. The acceleration of the sea breeze front which is indicated by the positive values is a result of the sea breeze flow combining with the valley flow. Since both flows are directed into the valley, the additive effect is to increase the speed of propagation of the sea breeze front, resulting in an earlier time of frontal passage at Salinas Airport. The large negative value was observed on 23 September 1987. This was a day in which the sea breeze front was diffuse in nature.

Table 9. EXAMINIATION OF THE LINEARITY OF THE SEA BREEZE FRONT: All times are Pacific Standard and in decimal hours.

Date	Monterey Bay Aquarium	Linearly Extrapolated Monterey Bay Aquarium	Δt	Monterey Airport	Linearly Extrapolated Monterey Airport	Δt
16				10.50	11.92	1.42
18				11.50	11.47	-.03
19	9.3335	10.50	1.17			
20	9.4166	9.49	.07	10.50	10.18	-.32
21	8.7501	8.22	-.53	11.50	10.59	-.91
22	8.7501	7.50	-1.25			
24				10.50	11.29	.79
26	9.4168	8.51	-.91			
29	9.0001	8.36	-.64	10.50	10.89	.39
30	9.7501	8.09	-1.66			

Table 10. EXAMINATION OF SEA BREEZE FRONTAL ACCELERATION: All times are Pacific Standard and in decimal hours.

Date	Fritzsche Field	Lineraly Extrapolated Fritzsche Field	Δt	Salinas Airport	Linearly Extrapolated Salinas Airport	Δt
16	10.50	10.36	-.14	11.50	12.59	1.09
18	10.50	10.26	-.24	11.50	11.56	.06
20				10.50	10.79	.29
21	9.50	9.76	.26	10.50	11.81	1.31
23				11.50	10.84	-.66
29	9.50	9.58	.08	11.50	12.25	.75
30	10.50	10.60	.10	11.50	11.46	-.04

VI. SUMMARY AND CONCLUSIONS

A. GENERAL FEATURES OF THE SEA BREEZE CIRCULATION

Observations of surface meteorological data on California's central coast during LASBEX showed a sea breeze circulation which was very similar to sea breeze phenomena observed in previous studies. In general, the sea breeze front was characterized by sharp discontinuities in wind direction, wind speed, temperature and humidity.

1. Observations Prior to Sea Breeze Frontal Passage

Prior to the passage of the sea breeze front, wind directions were highly variable changing from offshore to onshore flow. The wind speeds were light, decreasing to almost zero immediately prior to frontal passage. The air temperatures exhibited a gradual increase in the morning as a result of surface heating.

2. Observations at Sea Breeze Front Passage

With the passage of the sea breeze front the winds became onshore and up the Salinas Valley. The surface wind speeds showed a substantial increase as the front passed. During the majority of LASBEX observation days, the wind direction shift preceeded the increase in wind speed. The air temperatures peaked roughly at frontal passage and decreased somewhat as the sea breeze circulation was established. Relative humidity increased rapidly with frontal passage, leveling off as the day progressed.

The propagation of the front was examined using very simple linear geometry. The speed of propagation of the sea breeze front was

60

variable, ranging from 1 m/s to about 3 m/s, with a mean speed of
advance of 2 m/s±.54m/s. The direction of frontal propagation was to
the southwest with a mean propagation direction of $125°±26°$. The speed
of propagation of the sea breeze fronts observed during LASBEX was in
good agreement with previous observations reported by Simpson et al.
(1977) and Atkinson (1981). Fosberg and Schroeder (1966), investigating
the sea breeze in San Francisco Bay, found an initial speed of frontal
propagation of 2 to 4 m/s which increased to 5 to 7 m/s as the sea
breeze circulation interacted with the up-valley circulation. Olsson
et al. (1973), investigating a sea breeze event on Oregon's west coast,
found frontal propagation speeds in excess of 5 m/s. The faster
propagation speed is probably a result of topographic differences
between Oregon's coastal area and the Monterey Bay area. The coastal
ranges in western Oregon parallel the coastline and act as a barrier to
the inland penetration of marine air. The ranges are divided by
corridors which tend to funnel the marine air into interior valleys.
The convergence of the onshore flow in the corridors tends to increase
the speed of advance of the sea breeze front. In the Monterey Bay area,
the shape and elevation of the Salinas Valley topography results in less
of a funneling effect. The snyoptic weather patterns appear to be very
similar with high surface pressure situated off the coast. This does
not appear to be a contributing factor to the frontal speed disparities.

B. SURFACE HEAT FLUX OBSERVATIONS

During LASBEX, prefrontal surface heat flux estimates ranged from
100 W/m^2 to about 400 W/m^2. The scatter diagram of surface heat flux
versus speed of frontal propagation was generated to examine a possible

correlation between the speed of the front and the surface heat flux prior to the front's passage. The scatter diagram clearly shows that there is a positive correlation between the two. During the majority of LASBEX, an early morning stratus deck was present at the mouth of Salinas Valley. This is not uncommon for the Monterey Bay area during September. Radiosonde soundings were used to confirm that clouds were present at the mouth of the valley. The presence of clouds would change the fraction used to estimate the entrainment heat flux from the surface heat flux. The more clouds which are present the larger the estimating fraction. This would change the slope of the regression line through the data. However, the positive correlation would likely still exist.

C. LINEAR EXTRAPOLATION

The linear extrapolation of the sea breeze front was used to examine frontal acceleration. First, the deviations between the extrapolated arrival times and the observed arrival times at Monterey Bay Aquarium and Monterey Airport are believed to be a result of local topographic influence. The close agreement between the extrapolated and observed frontal passage times at Fritzsche Field indicates that the sea breeze front has not accelerated as it passed Fritzsche Field which is in close proximity to the initial observation triangle. Fritzsche Field is roughly 4 km east of the Marina Beach observation station and there are no major terrain differences between the stations. Finally, the arrival time differences observed at Salinas Airport are believed to be a result of the sea breeze front accele ' and decelerating. The sea breeze front accelerates down the Salinas Valley as it combines with the up-valley circulation which was generated by intense daytime surface

heating of the sloped ground. Through simple vector addition, the velocity of the sea breeze penetration joins the velocity of the up-valley flow yielding a faster moving sea breeze front. The observed superimposing of the sea breeze flow onto the valley flow is in good agreement with observations made by Fosberg and Schroeder (1977) and Olsson et al. (1973). The decelerating of the sea breeze front which was observed on 23 September was associated with a surface low pressure system which developed off California's central coast and disrupted the anticyclonic-cyclonic couplet which normally exists across the coastline. This is an area which lends itself to future investigation with a model which uses more complex geometry.

D. RECOMMENDATIONS

During LASBEX a large amount of data was acquired, most of which is awaiting analysis. An improved understanding of the relationship between coastal aerosol distributions, both horizontally and vertically, and the sea breeze is very important for the interpretation of coastal satellite imagery. Additional research is needed to understand the interactions of the sea breeze indigenous to California's central coast with the valley flow patterns. The microstructure of the sea breeze front is of special interest because the time height density of data from the experiment is better than in any previous studies.

LIST OF REFERENCES

Atkinson, B. W., 1981: Mesoscale Atmospheric Circulations. Academic Press, 495 pp. (see pp. 125-209).

Beers, Y., 1957: Introduction to the Theory of Error. Addison-Wesley Publishing Company, 66 pp. (see pp. 38-45).

Blair, T. A., and R. C. Fite, 1965: Weather Elements: a text in elementary meteorology. Prentice-Hall, 364 pp. (see pp. 128-129).

Dalu, G. A., and R. A. Pielke, 1989: An analytical study of the sea breeze. J. Atmos. Sci. Vol. 46(12), 1815-1825.

Fagan, M., 1988: The sea breeze circulation during the land sea breeze experiment (LASBEX) in Central California. M. S. Thesis, Naval Postgraduate School, Monterey, California, 127 pp.

Feliks, Y., 1988: A sea breeze front analytical ?del. J. Atmos. Sci. Vol. 45(6), 1030-1038.

Fosberg, M. A., and M. J. Schroeder, 1966: Marine air penetration in Central California. J. Appl. Meteor., 5, 573-589.

Frizzola, J. A., and E. L. Fisher, 1963: A series of sea breeze observations in the New York area. J. Appl. Meteor., 2, 722-739.

Huschke, R. E., 1986: Glossary of Meteorology, American Meteorological Society, 638 pp. (see pp. 275-276).

Hsu, S. A., 1988: Coastal Meteorology. Academic Press, 260 pp. (see pp. 140-147).

Intrieri, J. M., C. G. Little, W. J. Shaw, R. M. Banta, P. A. Durkee, and R. M. Hardesty, 1990: The Land/Sea Breeze Experiment (LASBEX). Bull.Am.Meteor.Soc., 71, 656-664.

Johnson Jr., A., and J. J. O'Brien, 1973: A study of an Oregon sea breeze event. J. Appl. Meteor., 12, 1267-1283.

Olsson, L. E., W. P. Elliott, and S. Hsu, 1973: Marine air penetration in western Oregon: an observational study. Mon. Wea. Rev., Vol. 101(4), 356-362.

Pielke, R. A., 1984: Mesoscale Meteorological Modelling, Academic Press, 612 pp. (see pp. 456-464).

Rotunno, R., 1983: On the linear theory of the land and sea breeze. J. Atmos. Sci. 40, 1999-2009.

Schroeder, M. J., M. A. Fosberg, O. P. Cramer, and C. A. O'Dell, 1967: Marine air invasion of the Pacific coast: a problem analysis. Bull. Amer. Meteor. Soc., Vol. 48(11), 802-807.

Shaw, W. J., and R. J. Lind, 1989: Sounding and surface meteorological data from the Land/Sea Breeze Experiment (LASBEX). Technical Report NPS-63-90-001, Naval Postgraduate School, Monterey, California, 293 pp.

Simpson, J. E., D. A. Mansfield, and J. R. Milford, 1977: Inland penetration of sea breeze fronts. Quart. J. Roy. Meteor. Soc., 103, 47-76.

Stull, R. B., 1976: The energetics of entrainment across a density interface. J. Atmos. Sci., 33, 1260-1267.

Walsh, J. E., 1974: Sea breeze theory and applications. J. Atmos. Sci. 31, 2012-2026.

Wexler, R., 1946: Theory and observations of land and sea breezes. Bull. Amer. Meteor. Soc., 27, 272-287.

Yan, H. and R. A. Anthes, 1987: The effect of lattitude on the sea breeze. Mon Wea. Rev., 115, 939-956.

INITIAL DISTRIBUTION LIST

No. Copies

1. Defense Technical Information Center   2
   Cameron Station
   Alexandra, VA 22304-6145

2. Library, Code 0142   2
   Naval Postgraduate School
   Monterey, CA 93943-5002

3. Chairman (Code 63Rd)   1
   Department of Meteorology
   Naval Postgraduate School
   Monterey, CA 93943-5000

4. Chairman (Code 68Co)   1
   Department of Oceanography
   Naval Postgraduate School
   Monterey, CA 93943-5000

5. Professor William J. Shaw (Code 63Sr)   12
   Department of Meteorology
   Naval Postgraduate School
   Monterey, CA 93943-5000

6. Professor Philip A. Durkee (Code 63De)   1
   Department of Meteorology
   Naval Postgraduate School
   Monterey, CA 93943-5000

7. Lt. Joseph A. Yetter, USN   2
   OA Division
   USS INCHON (LPH-12)
   FPO New York 09529-1655

8. Director Naval Oceanography Division   1
   Naval Observatory
   34th and Massachusetts Avenue NW
   Washington, D.C. 20390

9. Commander Naval Oceanography Command   1
   Stennis Space Center, MS 39529-5000

10. Commanding Officer   1
    Naval Oceanographic Office
    Stennis Space Center, MS 39522-5001

11. Commanding Officer   1
    Fleet Numerical Oceanography Center
    Monterey, CA 93943

12. Commanding Officer   1
    Naval Ocean Research and Development Activity
    Stennis Space Center, MS 39522-5001

13. Commanding Officer   1
    Naval Environmental Prediction Research Facility
    Monterey, CA 93943

14. Chairman, Oceanography Department   1
    U. S. Naval Academy
    Annapolis, MD 21402

15. Chief of Naval Research   1
    800 North Quincy Street
    Arlington, VA 22217

16. Office of Naval Research (Code 420)   1
    Naval Ocean Research and Development Activity
    800 North Quincy Street
    Arlington, VA 22217

17. Scientific Liaison Office   1
    Office of Naval Research
    Scripps Institution of Oceanography
    La Jolla, CA 92037

18. Library   1
    Scripps Institution of Oceanography
    P. O. Box 2367
    La Jolla, CA 92037

19. Library   1
    Department of Oceanography
    University of Washington
    Seattle, WA 98105